9-5-2013

Controlled Lasing in Gallium Nitride Nanowires

X Huiwen

Huiwen Xu

Candidate

Optical Science & Engineering - ECE

Department

This dissertation is approved, and it is acceptable in quality and form for publication:

Approved by the Dissertation Committee:

Ganesh Balakrishnan , Chairperson

Daniel F. Feezell

Sang M. Han

George T. Wang

Controlled Lasing in Gallium Nitride Nanowires

BY

Huiwen Xu

B.E., Communication Engineering, Hunan University, China, 2004
Ph. D., Computer Application Technology, Hunan University, China, 2010

DISSERTATION

Submitted in Partial Fulfillment of the
Requirements for the Degree of

Doctor of Philosophy
Optical Science & Engineering

The University of New Mexico
Albuquerque, New Mexico
July, 2013

Dedication

This work is dedicated to my beautiful wife, Jing Ju, and my lovely daughter, Evelyn Xu. It is also dedicated to my mother, Meizhen Pan and my father, Xianglin Xu.

ACKNOWLEDGEMENTS

I would like to express my deepest appreciation to my advisor, Prof. Ganesh Balakrishnan, for offering me opportunity to participate in his research group and conduct research under his guidance. His constant encouragement has helped me persevere through hard research problems with his expert guidance and insight.

I would like to acknowledge Dr. Qiming Li for co-advising me during my doctorial study. Working with him has been one of the most rewarding experiences of my life.

I would like to thank Dr. George Wang for his help and guidance.

I would like to thank Prof. Sang Han and Prof. Daniel Feezell for being a part of my committee.

I would like to thank my group members Jeremy Wright, Antonio Hurtado, Sheng Liu, and Changyi Li, for their inputs and fruitful discussion. I am extremely grateful for their friendship and spirit of teamwork.

I would like to thank Prof. Thomas Rotter, Chris Hains, Pankaj Ahirwar, Stephen Clark, Orlando, Emma, Sadhvikas and all the other group members for their supports.

In the end, I would like to thank my wife Jing Ju, my parents Meizhen Pan and Xianglin Xu, my in-laws, and my daughter Evelyn Xu for their love and supports.

Controlled Lasing in Gallium Nitride Nanowires

by

Huiwen Xu

B.E., Communication Engineering, Hunan University, China, 2004

Ph. D., Computer Application Technology, Hunan University, China, 2010

Ph.D., Optical Science & Engineering, University of New Mexico, 2013

Abstract

There is considerable interest in ultra-small coherent light sources. A strong candidate is a semiconductor-nanowire laser, where a single, monolithic nanowire functions simultaneously as an optical microcavity and active medium, leading to an extremely compact and robust laser. Recent advances in nanowire synthesis have enabled

realization of optically pumped nanowire lasers in different material systems, including III-V, III-nitride, and II-VI semiconductors. However, due to the limited lasing control techniques, most of the nanowire lasers operate in naturally-occurring multi-mode and randomly polarized states.

Lasing control in nanowire lasers is strongly desired for many practical applications. For instance, specifically polarized lasing is desired for atom trapping and biological detection, and single-mode lasing is crucial for applications needing high beam quality and spectral purity such as nanolithography and on-chip communications. Motivated by these practical requirements, this dissertation concentrates on the study of fundamental lasing characteristics and their control in gallium nitride (GaN) nanowire lasers.

GaN nanowire lasers typically operate in a combined multi-longitudinal and multi-transverse mode state. Two schemes are introduced here for controlling the optical mode and achieving single-mode operation of the nanowire lasers. The first method involves placing two nanowires side-by-side in contact to form a coupled cavity. The coupled cavity can generate a Vernier effect, which is able to suppress both multi-longitudinal and multi-transverse mode operation, giving rise to the single-mode lasing in these nanowire lasers. For the second method, single-mode lasing is achieved by placing individual GaN nanowires onto gold substrates. The nanowire-gold contact generates a mode-dependent loss, which can strongly attenuate high-order guiding modes and ensure single-mode operation.

Additionally, polarization properties of the gallium nitride nanowire lasers are studied experimentally by direct analysis of light emission from the nanowire end-facets. Linearly and elliptically polarized emissions are both obtained from a single nanowire at different pump strength, and a clear switching of the polarization states is observed with the change of optical excitation. This polarization change is attributed to a switching of transverse modes due to their difference in cavity losses.

Finally, lasing polarization control is allowed by the coupling of the GaN nanowire lasers to an underlying gold substrate. The gold substrate breaks the symmetry of the nanowire geometry and generates an inherent polarization-sensitive loss. These effects allow us to demonstrate linearly polarized emission of GaN nanowire lasers, with a large extinction ratio and a fixed polarization orientation parallel to the substrate surface.

Contents

List of Figures

List of Tables

Chapter 1

Introduction

1.1 The need for semiconductor nanowire lasers

Semiconductor nanowires are quasi-one-dimensional semiconductor structures, which by definition have cross-sectional dimensions from nanometers to hundreds of nanometers and lengths from hundreds of nanometers to millimeters. These subwavelength structures represent a new class of semiconductor materials for investigating light generation, propagation, detection, amplification, and modulation. In the recent two decades, semiconductor nanowires have witnessed an explosion of development, with tremendous of nanowire photonic devices demonstrated, including photodetectors[1,2,3,4], gas and biological sensors[5,6,7,8], waveguides[8,9], LEDs[10,11,12,13], mircodisplays[14,15], mircocavity lasers[16,17,18,19], solar cells[20,21,22,23] and nonlinear optical converters[24,25].

One of the most remarkable developments in this research area is the demonstration of lasing behavior in these nanowires. A semiconductor nanowire naturally satisfies the requirements of constructing a laser cavity, i. e., optical wave guiding, gain media, and the cavity feedback provided by the two end-facet reflection. As a nanowire is excited so that the optical gain balances the cavity loss, lasing will occur. After the first demonstration of lasing behavior in 2001[18], such miniaturized nanowire lasers have rapidly attracted intense attention in the research community since they have

exhibited a host of unique features compared to their planar counterparts. These include dislocation-free single crystalline nature, atomically smooth surface, one-dimensional geometry, wave-guiding ability, and large photon confinement.[26, 27]

Another appealing advantage of nanowires is their relaxed growth relationship to the substrate.[28,29,30,31] Nanowires can be grown either with or without an epitaxial connection to a substrate. For nanowires grown epitaxially from a substrate, the crystal orientation of the substrate is epitaxially transferred to the nanowires which determines orientation and direction of the nanowire growth. In this case, the requirement of lattice matching is substantially relaxed compared with the thin-film growth, and therefore a much larger strain can be tolerated. In the case of nanowire synthesis without epitaxial connection to a substrate, lattice matching requirement is further reduced where any substrate can be utilized for the nanowire growth. Such substrate insensitivity opens a wide material choices which are not available for planar growth. Moreover, the strain relaxation of the nanowire growth greatly enhances the toleration of lattice mismatch in semiconductor hetero-structures, highly enhancing design flexibility and performance of the hetero-structure based devices.

Besides the unique material properties, nanowire lasers have also exhibited attractive lasing characteristics and wide application potentials. Due to the ultra-short cavity length, the longitudinal resonance modes of nanowire lasers are largely separated, typically thousands times larger than that of microscopic lasers. This allows for the realization of single-mode nanowire lasers by simple geometry control of the nanowires.[32] The strong-guiding waveguide property also enables control of the nanowire

lasing characteristics by manipulating the evanescent fields of the propagation modes. As will be presented in this dissertation, longitudinal and transverse mode selection as well as polarization control of nanowire lasers can be achieved by controlling the evanescent fields of propagating modes.[33,34,35] The miniaturized dimensions of the nanowire lasers, and unique lasing characteristics, make them promising for tremendous groundbreaking applications, such as compact high resolution biochemical imaging, spectroscopy, atom trapping, integrated nanophotonics, nanolithography, high-resolution microdisplay, ultra-high density information storage, and localized excitation and detection.

1.2 Review of semiconductor nanowire laser techniques

Advances in semiconductor material synthesis have given rise to nanowires with controlled geometry and single-crystalline material quality, which enable the lasing behavior of such nanowires. After the pioneered works on nanowire lasing in ZnO[18] and GaN[17] nanowires by Yang's group, this research area has rapidly attracted intense attention and experienced a boost of development. Although there has been many works subsequently conducted on this area, they can be divided into two group: one has concentrated on nanowire synthesis aiming at high material quality and controlled nanowire geometry which enable the lasing behavior[36,37,38] , the other has focused on the study of the fundamental lasing properties and their control in nanowire lasers.

The bottom-up and top-down approaches are the two main categories for creating semiconductor nanowires.[27] The bottom-up approach builds up desired nanostructures starting with individual molecules or atoms. For nanowire synthesis, the bottom-up techniques include vapor-liquid-solid (VLS) chemical or physical vapor deposition, solid-

liquid-solid process, nanopore templating, and hydrothermal approaches.[27] Among these, the VLS growth, which promotes seeding and oriented growth by means of introducing a catalytic liquid alloy phase, has achieved the most success in synthesizing semiconductor nanowires in various material systems.[39,40,41,42] The growth of a crystal from direct absorption of a gas phase onto a solid surface is generally slow. The VLS mechanism circumvents this by introducing a catalytic liquid alloy phase which can rapidly absorb a vapor to supersaturation levels, and from which crystal growth can subsequently occur through nucleated seeds at the liquid-solid interface. The physical characteristics of nanowires grown in this manner depend, in a controllable way, upon the size and physical properties of the liquid alloy. The VLS technique was proposed in 1960s as an explanation for growing silicon whiskers from the gas phase with a liquid gold droplet placed on a silicon substrate as the catalyst.[43] After that, the technique has been developed for inorganic nanowire synthesis over the last two decades by Yang, Lieber, Samuelson, Hitachi, and many other research groups. This technique has given rise to the production of high quality nanowires, with the lasing demonstrated in a broad range of inorganic nanowires including GaN[17,44], CdS[16,45], CdSe[8,46], and ZnO[18,19].

The top-down approach bases on dimensional reduction of thin-film samples by means of mask-defined selective etch or nanoimprinting techniques. For the nanowire fabrication, the mask is commonly produced by Langmuir-Blodgett or lithographic techniques. Although being applied for fabricating silicon devices[47], the top-down technique has rarely been employed to produce III-V or II-VI semiconductor nanowires with lasing behavior until our efforts have been contributed. Our group in Sandia National Laboratories has developed a dry plus wet top-down etch approach to fabricate

GaN nanowires.[13,32] The approach involves a first step of assembling a close-packed monolayer silica microspheres on the surface of the GaN epilayer using Langmuir-Blodgett technique. This monolayer of silica microspheres functions as a mask layer for the subsequent inductively coupled plasma (ICP) etch, which forms an array of tapered GaN micro-pillars. Subsequently an anisotropic wet etch is used to selectively etch the GaN pillar sidewalls to form cylindrical (or hexagonal) and non-tapered GaN nanowires with desired diameters and to remove the plasma etch-damaged sidewalls. The nanowires fabricated using this technique have demonstrated high lasing performance, such as low lasing threshold, lasing capability with very short cavity, and lasing ability from arrays of them.

In addition to the advances in nanowire synthesis and fabrication, increasing efforts have been exerted on the fundamental lasing characteristics of such nanolasers. Due to the ultra-small cavity size, some principles obeyed by macroscopic lasers are not valid for these nanowire lasers. Also, new techniques need to be developed to control the nanowire lasing properties. Both theoretical and experimental efforts has been employed on nanowire lasers to illustrate the basis operation principles and to explore novel approaches to tailor the laser characteristics.

Cavity mode property, modal reflectivity, modal confinement and the far field distributions have been studied for nanowire lasers.[48,49,50,51] The cavity feedback of a nanowire laser is generated by the reflection from the two end-facets, which indicates a Febry-Perot cavity formed by a nanowire. Experimental results have confirmed the Febry-Perot cavity feedback for the nanowire lasers, where the longitudinal mode spacing obtained in the experiments agreed well with the calculated results.[50] Transverse modes

supported by a nanowire laser and their different reflectivities and far field properties have also been studied. Due to the small size of the waveguides, the reflectivities of the supported transverse modes differ with the conventional plane wave reflectivity determined by the Fresnel reflection formula $R=\left[\left(n_1-n_2\right)/\left(n_1+n_2\right)\right]^2$. To determine the reflectivities of different modes, the Maxwell equation needs to be resolved. Finite-difference time-domain (FDTD) method has been employed to solve this problem, revealing that that the reflectivity in the nanowire lasers varies with different modes.[49] Ning et al. have calculated the far field energy distributions of different transverse modes in a nanowire laser by using FDTD method in cylindrical coordinates.[48] It was found that HE_{11} mode gives rise to the maximum emission at $\theta=0$, while the transverse TE_{01} and TM_{01} modes cannot emit at $\theta=0$ and the emission maxima biased for 30^o ~50^o. The confinement factor is usually taken to mean the fraction of optical mode intensity contained within the active region. However, this is not accurate for semiconductor nanowire lasers due to the strong waveguiding. It has been shown for such strong waveguiding, the confinement factor can exceed unity.[51] This can be understand by taking the effective propagation distances of different modes into account for the effective gain calculation.

Direct evidence of transition from amplified spontaneous emission to coherent laser emission in optically pumped ZnO nanowires has been reported by Zimmler et al.[52] It has been described that the output power of the nanowire lasers experienced a transition from superlinear to linear regime when the pump power exceeded the lasing threshold. This lasing action has also been evidenced by the transition from uniform body

emission to directional emission along the nanowire and spectral Fabry-Perot modes exceeding the spontaneous emission background by orders of magnitude.

Different approaches have been proposed or demonstrated for reducing the lasing thresholds of nanowire lasers. The basic idea is to reduce the cavity loss by enhancing the cavity feedback, which typically is generated from the nanowire end-facet reflection with a reflectance of ~20%. In 2006, Pauzauskie et al. developed a nanowire ring laser by bending a nanowire and connecting the two emission ends. [53] The ring cavity alleviates the cavity loss from the end emission and leads to a low lasing threshold of 75 $\mu J/cm^2$. Additionally, they demonstrated significant changes in nanowire photoluminescence, Q factor, and lasing modes by manipulating a linear nanowire into the ring geometry. Following the side-by-side coupling of nanowire ends, peak emission wavelengths shift by nearly 10 nm due to improved coupling efficiency between tangentially overlapping nanowire ends, Q factor enhancement, and preferential gain in long-wavelength modes. In 2006, Chen et al. proposed a nanowire structure with distributed Bragg reflector at the two nanowire ends for enhancing the end-facet reflectivity and thereby reducing the threshold of these lasers.[54] Their simulation results show that the geometry has advantages as threshold reduction, enhanced stimulated emission over spontaneous emission and support of single wavelength operation.

Different approaches have been developed to achieve single-mode operation in nanowire lasers. The first single-mode nanowire laser was realized by Tong's group in 2011.[46] The single-mode lasing was achieved by folding a long CdSe nanowire to a "figure-8" shape. The "figure-8" nanowire forms a coupled cavity, which is able to enlarge the longitudinal mode spacing of the cavity and thereby reduce the lasing modes.

Taking use of the same mechanism, single-mode lasing from a 'X-shaped' coupled nanowire cavity was also obtained.[55] The coupling effect was also demonstrated in a cleaved nanowire geometry.[56] In this geometry, two end-to-end nanowires were formed by cleaving a single nanowire using focus ion beam mining. By controlling the cleaved gap, the coupling loss was minimized while strong coupling from one nanowire to the other could be generated. As-fabricated single-mode lasing has also been realized in GaN nanowire lasers, where the single-mode operation was ensured by the precise control of the nanowire length and diameter during the fabrication process.[32] Since GaN nanowires typically operates in a combined multi-transverse and multi-longitudinal mode operation, they both need to be suppressed to achieve single-mode lasing. In this work, the GaN nanowire diameter was reduced to ~130 nm so that the nanowire functioned as a single-mode waveguide, which bypassed the multi-transverse mode operation. Multi-longitudinal mode operation was suppressed by reducing the nanowire length to ~5 μm, which strongly enhanced the mode competition and generated the single-mode lasing. Although capable of generating as-fabricated single-mode nanowire lasers, this technique is restricted to nanowire with very small dimensions, which has the drawbacks of reduced gain volume and mode confinement, and surface defect effects due to the large surface-volume ratio, leading to an increased lasing threshold.

To address this limitation, we have developed a method that uses a nanowire-pair geometry to generate single-mode lasing for GaN nanowires with larger dimensions.[33] The nanowire-pair was formed by putting two nanowires side-by-side in contact. A coupling effect can be generated from the nanowire-pair, which is able to not only select longitudinal mode, but also suppress the multiple transverse mode oscillation in the

cavity. Single-mode lasing in GaN nanowires with diameters as large as 800 nm has been achieved by this approach. We have also demonstrated that a transverse mode can be selected by coupling a nanowire to a gold substrate.[34] The nanowire-gold contact generates a mode-dependent loss, which strongly attenuates higher transverse modes and ensures single-mode operation.

Large band wavelength tuning has also been realized in nanowire lasers.[57] By selectively pumping a certain fraction of a nanowire instead of uniformly pumping the whole nanowire, the lasing wavelength of a nanowire laser can be shifted. Over 30 nm tuning range has been achieved by such selective pumping in a CdS nanowire laser. This tuning effect is attributed to the combine effects of self-absorption, band renormalization and pulling effect. Similar results have been reported in a CdSe nanowire, with a wavelength tuning range of ~40 nm.[58] The wavelength tuning has been argued as a result of self-absorption effect from the unpumped nanowire section, which tends to absorb the light with short wavelength, thereby shifting the lasing wavelength.

1.3 Introduction to gallium nitride

GaN is a binary III/V direct bandgap semiconductor, and one of the most important semiconductor materials since silicon. GaN and its III-N alloys (AlGaInN) have established themselves as exceptionally significant semiconductors for short wavelength optoelectronics, and high frequency, high power electronics. The main reason for that is due to their direct energy band gaps covering the entire visible and a large part of ultra-violet spectral range. Also, the large band gap and high chemical and thermal stability allow them to be used in harsh environments.

Group III-nitrides can crystallized in zinc-blende (cubic) or wurtzite (hexagonal) polytypes. The wurtzite III-nitrides are more interesting since wurtzite GaN, AlN and InN all have direct bandgaps, with the room-temperature band gap energy of 3.39, 6.2 and 0.8 eV respectively. The compounds of III-nitride semiconductor potentially cover the emission range from deep ultra-violet to near infrared. The large band gap of GaN also gives rise to a low sensitivity of intrinsic carrier concentration on the temperature, which leads to a much higher device stability compared with silicon and GaAs based semiconductor materials. In addition, the wurtzite III-nitrides are highly piezoelectric, offering promising for device designs which cannot be accessed by common Si or GaAs based semiconductors. Furthermore, GaN has strong absorption and optical gain coefficients of 40000 cm^{-1} and 7200 cm^{-1} respectively, making it a good candidate for short wavelength photodetectors and light emitting sources.

III-nitrides can be used in many electronic and optoelectronic applications. One significant application is emitting brilliant light in the form of light emitting diodes (LEDs) and laser diodes. LEDs play an important role in general lighting, luminescence displays, including traffic lights, and television and cell phone backlights. The unique features of the LEDs, such as high efficiency, long lifetime and quick response time, make them the ultimate general source of continuous light. GaN-based laser diodes are also used for high capacity optical storage applications. Since the resolution of optical reading and writing is reversely proportional to the laser wavelength, the CD capacity can be expanded from 0.8 GB (780 nm operation wavelength for CDs) and 4.7 GB (650 nm operartion wavelength for DVDs) to over 25GB by using the UV lasers. Additionally, UV laser diodes also are finding applications in biochemistry and medical sciences. GaN

is also the key material for next generation high frequency, high power transistors capable of operating at high temperatures. For example, GaN is the substrate which makes violet (405 nm) laser diodes possible, without use of nonlinear optical frequency-doubling. Because GaN transistors can operate at much higher temperatures and work at much higher voltages than gallium arsenide (GaAs) transistors, they can make ideal power amplifiers at microwave frequencies. Furthermore, AlGaN/GaN HEMTs have demonstrated excellent characteristics, paving the way for high-efficiency operation of high power GaN HEMTs for amplifiers of next-generation mobile base stations.

1.4 Organization of the dissertation

In this dissertation, the fundamental lasing properties are studied and several unique techniques are introduced for controlling such lasing properties, including the mode selection and polarization control. The dissertation is organized as follows.

Chapter 1 gives the introduction of the nanowire lasers in terms of motivation of nanowire laser study, and state-of-art techniques for nanowire synthesis and lasing control. The material properties of GaN are also introduced.

Chapter 2 is devoted to the fundamental operation principles for the nanowire lasers. The chapter mainly focuses on the novel operation features of these nanolasers which differ with those of the conventional lasers. These include the extremely large longitudinal mode spacing, and different cavity feedback, modal gain and far field properties for different transverse modes.

Chapter 3 introduces the experimental and simulation techniques used in the dissertation to fabricate, characterize and analyze the nanowire lasers. A dry plus wet two-step top-down etch approach is introduced to fabricate the nanodevices with high material quality and controlled geometry. The nanodevices are optically characterized by means of mirco-photoluminescence setups. A specific dual-arm mirco-photoluminescence setup is developed to characterize the laser emission directly from the nanowire end-facets, which enable the analysis of the nanolaser polarization and far field properties. A commercial software package based on FDTD technique is employed for the analysis of the nanowire properties.

Chapter 4 presents a technique developed for realizing single-mode operation in GaN nanowires by placing two nanowires side-by-side in contact. The single-mode lasing is achieved by a coupling effect between the two nanowires, which generates a much more restricted resonance condition and thereby dramatically reduce the lasing mode in the coupled cavity.

Chapter 5 proposes an alternative approach to achieve single-mode lasing from individual GaN nanowire lasers. This is realized by simply coupling a nanowire to a underlying gold substrate. The gold substrate generates a mode-dependent cavity loss, which can suppress all the high-order modes from oscillating in the cavity and ensure the single-mode operation.

Chapter 6 studies the polarization properties of the GaN nanowire lasers. It is found that one single nanowire can lase with different polarization states when the optical excitation strength is changed. A clear polarization state switching from linear to

elliptical is measured experimentally. This phenomena is attributed to a transverse mode switching due to their different cavity feedbacks.

Chapter 7 presents an approach to control the polarization of nanowire lasers by coupling them to a gold substrate. In addition to suppress high order transverse modes, the metal substrate can generate a polarization-dependent loss, which ensures the linear polarized laser emission with the polarization clamped parallel to the substrate surface.

Chapter 8 discusses conclusions and future directions.

Chapter 2

Theoretical Fundamentals for Nanowire Lasers

Regardless of the constructed material, the general operation principles for nanowire lasers are similar. To enable the lasing behavior, the key factors for a laser cavity need to be satisfied, which include optical gain, waveguiding, and cavity feedback. Interestingly, an as-fabricated semiconductor nanowire naturally fulfills these requirements. A free standing nanowire typically has a circular (hexagonal or triangular) cross-sectional geometry, where the refractive index of the semiconductor material is much larger than that of the surrounding air forming an effective waveguide. The high refractive index difference between the semiconductor material and the surroundings allows for efficient waveguiding even when the nanowire cross-sectional size is comparable to or even smaller than the operation wavelength. The cavity feedback is provided by the reflection of the guided modes from the nanowire end-facets, which forms a micro-sized Febry-Perot cavity. When a nanowire is excited, carriers can be injected in the nanowire which provides the material gain for the laser operation.

However, the miniaturized dimension of the nanowires lead to many interesting difference in principles compared to those for the macroscopic lasers. For instance, the

small transverse dimension of a nanowire generates propagation modes with a considerate portion of light fields outside the waveguide, which results in the invalidation of Fresnel rules which dominates the typical diffraction problems of guide wave scattering upon discontinuity. For the same reason, the far field property and the modal confinement also need to be reevaluated. To address these problems, Maxwell's equations need to resolved, which is best approached by numerical methods. This chapter will describe some theoretical aspects of nanowire lasers, especially those distinguishing them from other existing lasers.

2.1 Cavity feedback

Lasing occurs in a nanowire when the injected carriers provide sufficient gain to balance all the cavity losses. Since a nanowire cavity feedback is generated by the reflection from the two end-facets, it naturally forms a Febry-Perot laser cavity. Therefore, the threshold equation for a free-standing nanowire laser can be presented as[50]:

$$\Gamma g_{th} = \alpha_t$$
$$\alpha_t = \alpha_R + \alpha_W \ ,$$
$$\alpha_R = \frac{1}{L}\ln\frac{1}{R}$$

Where Γ is photonic confinement factor, g_{th} is the threshold material gain (Γg_{th} is the modal gain), L is the nanowire length, R is the end-facet reflectivity, and α_t, α_R, α_W stand for total loss, end-facet reflection loss, and wave guiding loss coefficients, respectively. Although the end-facet reflectance and the waveguide loss due to scattering both contribute to the cavity loss, the end-facet loss dominates in typical nanowire lasers

due to the low reflectivity at the nanowire-air interfaces.[50] These equations render the relationship between the cavity length, mode confinement and the lasing threshold in the following way: large cavity length and confinement factor lead to a low threshold; on the contrary, small cavity length and mode confinement result in a high threshold. Since the nanowire waveguide is formed by refractive index contrast between the semiconductor material and the surrounding air, the mode confinement is intensely related with the nanowire cross-sectional dimension, i. e., for a given propagation mode, the mode confinement increases as the nanowire diameter increases. Therefore, a nanowire with larger diameter and length is believed to have a lower lasing threshold.

2.2 Longitudinal modes

A nanowire laser commonly has a Febry-Perot cavity, where the resonance occurs when the phase of a light wave constructively interfere with itself after a round trip propagation inside the cavity. This resonance condition gives a longitudinal mode spacing determined by

$$\Delta\lambda = \frac{1}{L}\left[\frac{\lambda^2}{2}\left(n(\lambda) - \lambda\frac{dn(\lambda)}{d\lambda}\right)^{-1}\right],$$

where L is the cavity length (or nanowire length), λ is the wavelength and $n(\lambda)$ is the refractive index at the wavelength λ. This equation indicates that the longitudinal mode spacing is reversely proportional to the nanowire length and the spacing at different wavelength may not be even due to the dispersion of the refractive index. As an example, Fig. 2.1 describes the dependence of nanowire length of the above-threshold laser spectra

obtained from different ZnO nanowires.[50] Fig. 2.1(a) shows the lasing spectra experimentally obtained for three nanowires with different lengths. The observed sharp spikes corresponds to the longitudinal lasing modes of the nanowire cavities. It is seen that the mode spacing decreases with the increase of the nanowire length. In addition, for each spectrum obtained from a given nanowire, the mode spacing in the long wavelength side is larger than that in the short wavelength side, indicating a negative dispersion of the refractive index for this material. It is further evidenced in Fig. 2.1(b) that the reversely proportional relationship between the mode spacing and the cavity length, where the mode spacing at the same wavelength is measured for nine nanowires with different lengths.

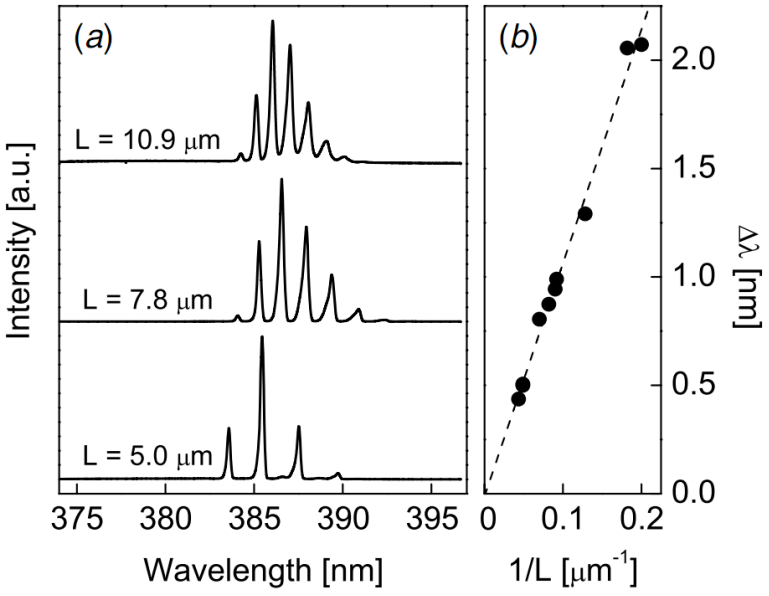

Figure 2.1 Nanowire length dependence of above-threshold laser spectra from ZnO nanowires. (a) Laser oscillation spectra for three nanowires of different lengths; (b) Spacing between adjacent modes versus 1/L. (figure taken from [50])

2.3 Transverse modes

The single-mode operation of circular waveguides is roughly determined by the equation $(\pi D/\lambda)\left(n_1^2-n_0^2\right)^{0.5}<2.405$, where D is the nanowire diameter, λ is the wavelength in vacuum, and n_1 and n_0 are the refractive indices of the nanowire and the surrounding air, respectively.[59] It is seen that the single-mode cutoff diameter depends on the operation wavelength and the refractive indices of the semiconductor and the surrounding materials. Since the most demonstrated semiconductor nanowires have refractive indices from 2.5~3 and the surround material is air for most cases, the operation wavelength becomes the dominating factor for the cutoff diameter. For the nanowires operating in short wavelength regime, such as GaN and ZnO nanowires, the cutoff diameter for them to behave as single-mode waveguides is in the range of 120~150 nm. Therefore, the nanowires with larger transverse dimensions guide multiple modes. Here, one question is raised that whether a specific mode is favored for lasing in these nanowire lasers. To address this issue, analysis needs to be conducted on the reflectivity, modal gain, far field characterization of these nanowires.

2.4 Reflectivity of different transverse modes

The reflectivity at the interface of two different material is usually determined by the Fresnel reflection formula $R=\left((n_1-n_0)/(n_1+n_0)\right)^2$, where n_1 and n_0 are the refractive indices of the materials on the two sides of the discontinuity. However, this formula does not apply for the nanowire lasers. Since the guiding modes are partially confined within the nanowires, only a fraction of the modes experience the end-facet reflection. As can be seen that the modal properties will have a strong effect on the end-facet reflectivity. To

accurately analyze the reflectivity of guided modes, Maxwell's equations need to be numerically resolved. FDTD method can be used to calculate the reflectivity. In this approach, the transverse modes supported by the cross-sectional geometry is firstly calculated, and then these modes obtained can be separately employed for the following reflectivity calculation. Fig. 2.2 shows an example of calculated reflectivities for guiding modes supported by a ZnO nanowire on SiO_2 substrate geometry.[49] This structure supports modes that closely resemble the transverse electric (TE_{0m}), transverse magnetic (TM_{0m}) and hybrid (HE_{nm}) modes typically found in a cylindrically symmetric case of a free standing nanowire. Differently, the presence of the substrate breaks the cylindrical symmetry of the problem, rendering the calculation tractable only numerically. In addition, the substrate distorts the modes by pulling the field into the substrate. It is seen from the figure that only HE_{11} mode exists when the nanowire diameter is in the range of 100~160 nm, and its end-facet reflectivity is less than 20%. When the nanowire diameter reaches 170 nm, the nanowire starts to support the TE_{01} mode; and when the diameter reaches 220 nm, it supports both TE_{01} and TM_{01} modes. Interestingly, the TE_{01} and TM_{01} modes show larger laser reflectivity compared to that of the HE_{11} mode in this case. For the TE_{01} mode in specific, the reflectivity can be as high as about 45%, which is over two times larger than that of the HE_{11} mode. The simulation results suggest that for regular ZnO nanowire with diameter in the range of 200~400 nm, The lasing threshold for the TE_{01} and TM_{01} modes should be less than the HE_{11} mode, thereby be favored to lase in such nanowire lasers.

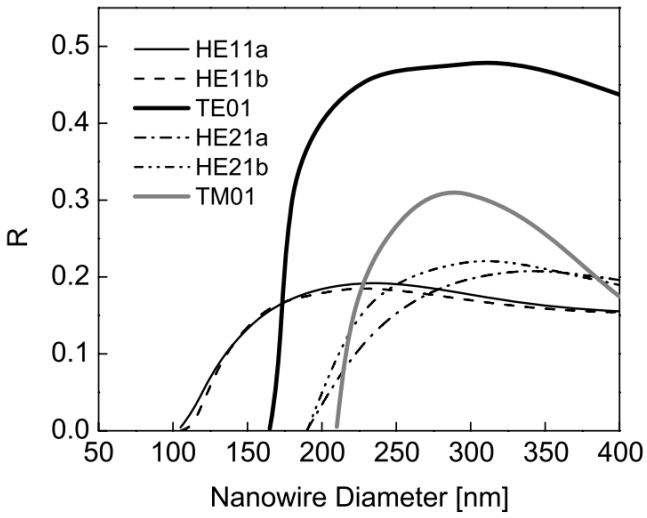

Figure 2.2 Reflection coefficient for several lowest-order modes of a ZnO nanowire lying on a silica substrate. (figure taken from [49])

2.5 Far field

While nanowires with small diameter support only HE_{11} mode, nanowires with larger diameters can support higher order modes, such as TE_{01} and TM_{01}. The mode types are typically distinguished by comparing the lasing spectral peaks according to their different dispersion properties. However, this approach may be ambiguous since different modes may have the similar lasing wavelengths which may not be distinguished by a common spectrometer. The far field analysis may offer a better solution to the problem, where the mode profile and polarization can be analyzed for confirming the mode type. To describe this the situation is considered that the radiation originates from the end of a free-standing nanowire. This is a typical diffraction problem that is similar to that of optical fibers which have been studied thoroughly. However, the strong guiding property of a semiconductor nanowire make it differ with the fiber case, and therefore the obtained far-

field results for fibers does not apply for the nanowires. FDTD method can be employed to calculate the far-field emission of a nanowire laser.[48] This is typically conducted by calculating the supported modes by the transverse geometry and then calculating the propagation of a certain mode after it reach the end-facets, which give rise to the time-dependent fields in the far-field region. Fig. 2.3 shows a calculated result of far filed energy density as a function of θ for the three lowest modes supported by a multimode waveguide: TE_{01}, TM_{01} and HE_{11} modes.[48] For the HE_{11} mode, the emission at small θ is quite large and is independent of polarization. As $\omega R/c$ increases, the forward emission decreases while the backward direction increases. The broadening of the emission angle with the increase of $\omega R/c$ can be understood as the decrease of the transverse extent of the mode for larger $\omega R/c$. Also, when $\omega R/c$ is small, a strong maximum at $\theta = 0$ is achieved. This can be attributed to the weak localization of guided modes in thin nanowires. However, the reflection from the end facet is small correspondingly, which results in a high threshold gain. Thicker nanowires can provide lower threshold while their emission has a broader angular distribution.

The emission for the transverse TE_{01} and TM_{01} modes shows large difference from that of the HE_{11} mode. As shown in Fig. 2.3(a), the emission is complete absence at $\theta = 0$. This is the direct result of the symmetry of these modes. For a mode having far field at $\theta = 0$, it must have electric and magnetic fields perpendicular to the nanowire axis, which cannot be produced by the TE_{01} and TM_{01} modes.

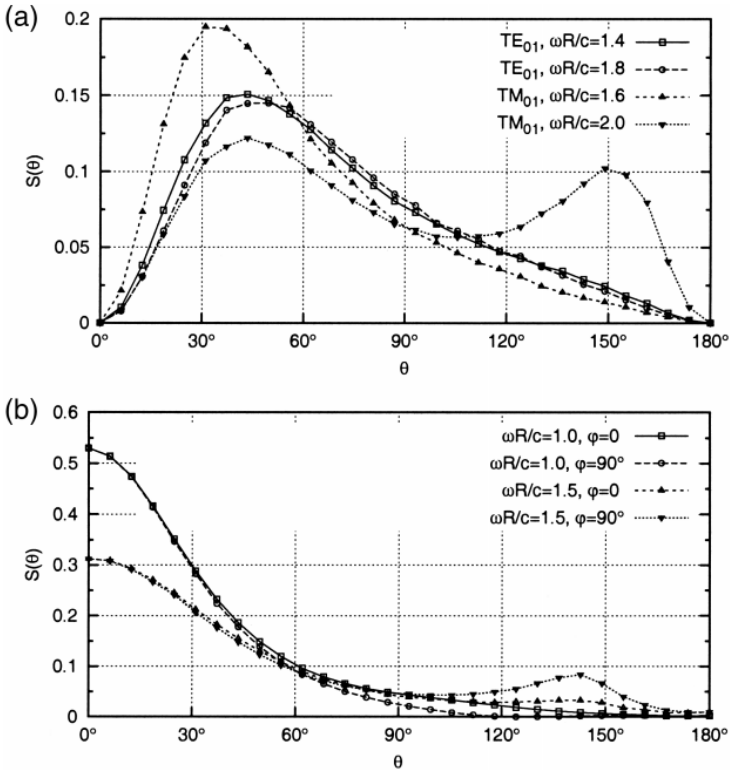

Figure 2.3 Normalized far-filed intensity as a function of for (a) TE_{01}, TM_{01} and (b) HE_{11} modes. (figure taken from [48])

Chapter 3

Fabrication, Characterization and Simulation Techniques for GaN Nanowires

This chapter introduces the experimental and simulation approaches used in the dissertation to fabricate, characterize and analyze the III-nitride nanowire lasers. A novel top-down two-step etch technique is introduced, which is developed by our group in Sandia National Laboratories for the fabrication of the III-nitride nanowires and other nanostructures. The fabricated nanostructures are characterized using micro-photoluminescence (μ-PL) setups. In addition to the one-arm μ-PL setup, a technique commonly employed for the nanowire characterization, we develop a dual-arm μ-PL setup to analyze the light emission directly from end-facets of nanowires. The dual-arm μ-PL setup allows for precisely analyzing the polarization and far field pattern of the nanowires. A commercial software package based on FDTD technique, "Mode Solutions", is used for analyzing the nanowire operation, including the guiding mode analysis, propagation loss, and far field property analysis.

3.1 Fabrication of GaN nanowires

Figure 3.1 The main steps of the top-down etch technique for fabricating GaN nanostructures.

A unique top-down dry-plus-wet etch technique is developed in our experiment to fabricate GaN-based nanowires and other nanostructures.[32] This technique is able to fabricate nanostructures with single crystalline material quality, controlled geometry and smooth surface. The fabrication process involves four main steps as seen in Fig. 3.1. This process starts with a c-plane GaN epitaxial thin film, which is grown in a metalorganic chemical vapor deposition (MOCVD) reactor on a 2 inch sapphire substrate. After the GaN growth, a mask layer is deposited on the surface of the GaN epilayer serving for the following dry etch. Depending on the desired device structure, two different techniques are utilized for producing the etch mask, i. e., one way is to utilize Langmuir-Blodgett techniques to form a close-packed monolayer of silica microspheres which is able to define arrays of cylindrical nanowires; the other way is to use e-beam lithography technique to define arbitrarily shaped masks for making devices with flexible geometries.

Subsequently, the mask geometry is transferred into the epilayer by the inductively coupled plasma dry etch, with the etch depth controlled by the duration of the dry etch. After the dry etch, tapered-shaped nanostructures are formed with severe surface damage and roughness. An anisotropic AZ400K-based wet etch is thereby utilized to selectively etch the structures to get straight and smooth sidewalls, which give rise to the improved optical performance of them.

3.1.1 Mask design and fabrication

A etch mask is a material that blocks etching in selected areas of the substrate surface, which defines the resulting surface morphology after the etch process. In order to fabricate cylindrical nanowire structures, etch mask utilized needs to have a circularly shaped cross-section. For this purpose, Langmuir-Blodgett technique is employed to generate a close-packed monolayer of silica microspheres. To define arbitrarily shaped or spaced etch mask, the electron-beam lithography technique can be used. These two techniques are detailed as follows.

Single monolayer microsphere deposition on the GaN epilayer is achieved by using a Langmuir-Blodgett trough, which is a laboratory apparatus used to compress monolayers of molecules or particles on the surface of a given subphase and measure the surface phenomena due to this compression so as to deposit single monolayer of the molecules to a given substrate.[60,61] Fig. 3.2 illustrates the process of the Langmuir-Blodgett deposition.[62] Firstly, the molecules to be deposited are dispersed onto the surface of a sub-phase, typically oriented with the hydrophobic part upwards and with the hydrophilic part immersed in water. The surface area occupied by each molecule is

subsequently compressed by means of the movement of barriers in order to produce a highly densely packed array of the molecules in a solid state. The molecule transfer to a properly cleaned and prepared solid substrate can be performed from this state by dipping and lifting the substrate through the condensed Langmuir layer. To ensure the solid state is maintained during molecule transfer from the sub-phase to the substrate, a continuous movement of the barriers is performed which is monitored by a surface tension sensor.

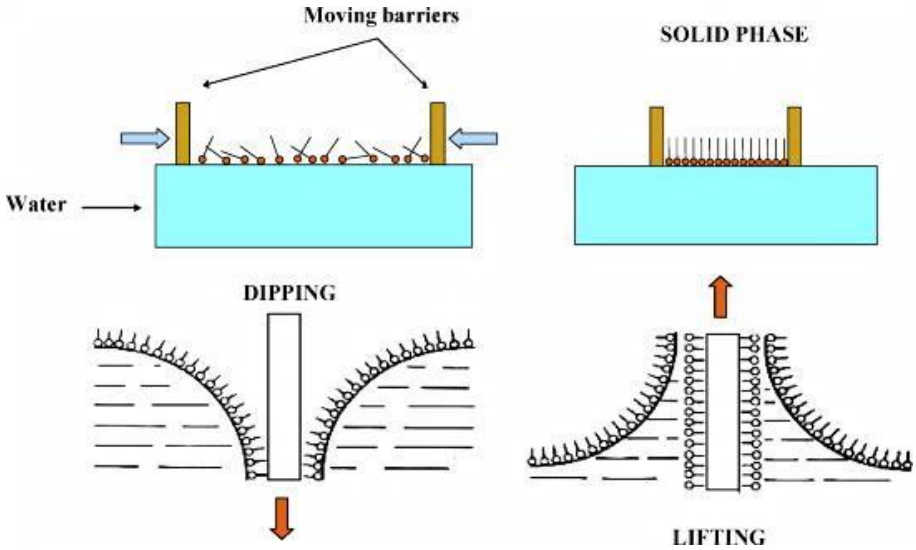

Figure 3.2 Schematic representation of the Langmuir-Blodgett deposition procedure. (figure taken from [62])

In particularly, to fabricate 2-dimensinal array of circularly cross-sectional masks for the nanowire array generation, 1~5 μm silica microspheres and distilled water are employed as the particles to be deposited and the subphase respectively. The monolayer of silica microspheres is assembled on a GaN epilayer following a process reported by Reculusa and Ravaine[60]. Firstly, given amounts of silica microspheres are introduced into an ethanol and ammonia solution. Sonication of the mixture solution is then performed to

homogenize it. Second, a large excess of allyltrimethoxysilane is added to functionalized the silica surface. This mixture is then sonicated at a system temperature of 90 ^{o}C for two hours in order to gain proper hydrophobicity for the spheres which prevents the aggregation phenomenon of the spheres from occurring. Thirdly, to eliminate the remaining reagents, the suspension is dialyzed several times and then transferred to a flask under continuous stirring. Fourth, after a few times purification by absolute ethanol, the suspension is then redispersed in a 8:2 mixture of chloroform and ethanol and sonicated for several minutes. Finally, this suspension is carefully spread along the water surface of the Langmuir trough, and a condensed single-layer is formed at a surface tension of 11 $mN \cdot m^{-1}$ when sphere transferred starts with the dipping and lifting of the GaN substrate.

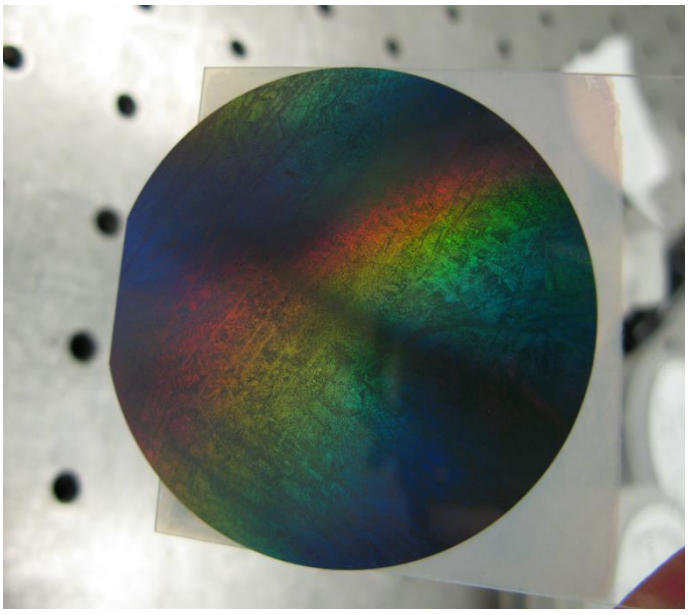

Figure 3.3 Optical image of silica substrate deposited with a monolayer of 3 μm silica microspheres.

Using the Langmuir-Blodgett technique, we successfully demonstrate monolayer microsphere deposition on various substrates (e.g. GaN, glass, silica) with different sphere diameters (1 μm~5 μm). Fig. 3.3 shows an image of 2 inch silica wafer coated with a monolayer of 3 μm microspheres. A colorful diffraction pattern can be seen on the sample surface from proper observation angles when the sample is illuminated by a lamp, indicating the generation of uniformly packed two-dimensional array of the microspheres.

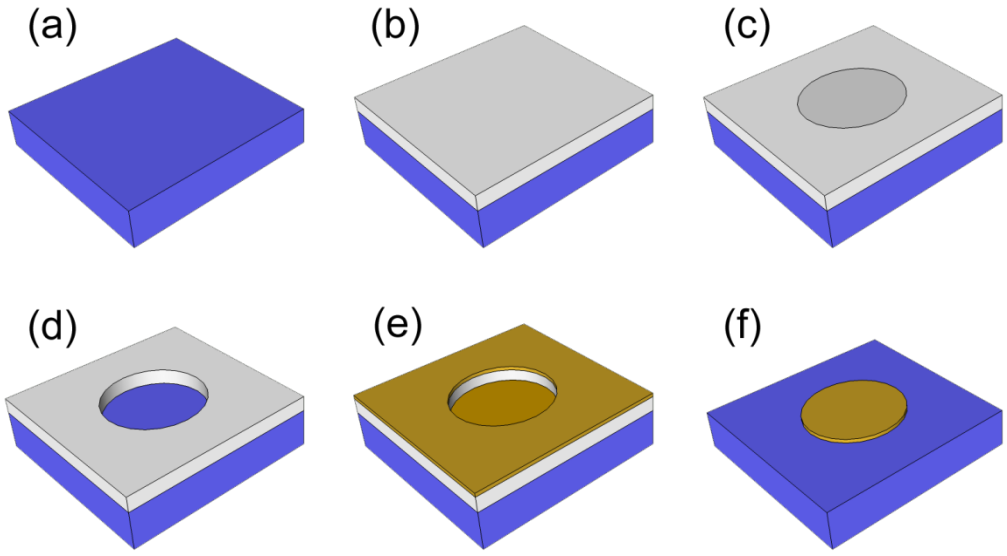

Figure 3.4 Schematic of the electron beam lithography procedure. (a) GaN substrate; (b) PMMA coated on the GaN substrate; (c) electron beam patterning (circle indicates the exposed region); (d) development performed in a 1:3 MIBK to IPA solution; (e) metal deposition; (f) metal mask obtained after removal of the rest PMMA and the metal attached to it.

While the Langmuir-Blodgett technique can produce masks with two-dimensional arrays of microspheres, electron beam lithography technique is able to define arbitrarily shaped masks. Electron beam lithography is the practice of emitting a beam of electrons

in a patterned fashion across a surface covered with a layer of resist, and of selectively removing regions of the resist. Depending on the resist type, either exposed (for positive tone resist) or non-exposed (for negative tone resist) region can be removed. In our experiments, polymethyl methacrylate (PMMA) is used as the resist. The PMMA is a positive tone resist, indicating the removal of the exposed region after the electron beam writing.

Fig. 3.4 sketches the process of mask fabrication by the electron beam lithography technique in our experiment. Firstly, a layer of PMMA is deposited on the GaN surface by spin coating (Fig. 3.4(b)). The thickness of the PMMA resist is determined by the solid PMMA concentration of the resist and the spin speed. Higher solid concentration leads to a thicker layer, and for a given solid concentration, higher spin speed gives a more uniform but thinner PMMA layer. In our experiment, a commercial resist 950PMMA-C2 from Microchem Inc is commonly used which has 2% of the PMMA solids in chlorobenzene. A spin speed of 4000 rounds per minute is used to generate a uniform PMMA layer with the thickness of ~ 300 nm. This sample is subsequently loaded into a scanning electron microscope from FEI Inc for the electron beam exposure (Fig. 3.4(c)). An electron beam current of 520 pA and an intensity dose of 350 $\mu C/cm^2$ are employed for the PMMA resist exposure. After the exposure, the exposed regions can be selectively removed by placing the sample into the 1:3 methyl isobutyl ketone (MIBK) to isopropanol (IPA) developer for about one minute (Fig. 3.4(d)). The development is stopped by moving the sample to a pure IPA solution for another one minute. Subsequently a metal layer with the thickness of ~100 nm is deposited to the sample surface by using electron beam evaporation (Fig. 3.4(e)). At last, the residual PMMA and

the metal on top of it are removed by dipping the sample to a acetone solvent, leaving only the metal mask on the electron-exposed region (Fig. 3.4(f)). The resolution for the metal mask by the electron beam lithography is ~50 nm, which is affected by the thickness of the PMMA layer, the deposited metal thickness, the resolution of electron beam scanning, and the duration of the development.

Compared with the Langmuir-Blodgett technique, electron beam lithography has more flexibility to make masks for single devices. Due to the high resolution and flexible mask shape control, it is desired for fabricating nanostructures with geometries that could not be formed by regularly shaped masks. For example, this technique has been used in our experiments to fabricate hexagonal microdisks, nanospirals, and coupled nanorings. On the other hand, this technique typically limits the produced metal mask thickness to be only a few hundreds of nanometers, which prevents it being used for applications needing large etch depth, such as fabricating vertically oriented long nanowires. In addition, the electron beam exposure process is time consuming that may not be suitable for large scale patterning to make dense nanostructures on a single wafer.

3.1.2 Two-step top-down etch

A unique two-step “dry plus wet” etch technique is utilized to transfer the mask pattern into the GaN epilayer. Due to the circularly cross-sectional geometry, the monolayer of silica microspheres prepared by means of the Langmuir-Blodgett technique is suitable to function as the mask to fabricate nanowire arrays. Fig. 3.5(a) sketches the geometry of a monolayer assembled on a GaN epilayer, and (d) shows a corresponding top-view SEM image from a real sample. The etching process starts with a inductively coupled plasma

(ICP) dry etch. The ratio of the etch rates for the silica spheres and the GaN substrate is ~ 1:2, indicating an obtainable etch depth of ~ 6 μm on the uncovered GaN substrate by using 3 μm diameter spheres. We also notice that the spheres shrink during the dry etch process. Therefore, the etch duration needs be precisely controlled so that residual silica spheres have diameters of about a few hundreds of nanometers, which defines the top dimension of the resulting nanoposts. The gradual shrinking of the spheres, together with the shadow effect for the ICP etch, give rise to the formation of nanopost arrays with strong tapered shape, as indicated by Fig. 3.5(b) and (e). Moreover, many surface defects are formed after the dry etch, which leads to a severe surface scattering, preventing the effective waveguide of the nanoposts from happening. This is confirmed experimentally that no laser emission is obtained from these nanoposts when optically excited. To address this issue, a following wet etch process is employed to remove the surface damage and generate nanowires with uniform and straight sidewalls[13]. The wet etch is performed in a AZ400K (KOH based) developer with a system temperature of 65 ^{o}C. The wet etch is an anisotropic process which does not affect the C-plane surfaces and has a relatively lower etch rate for M-plane surfaces of the GaN material. Therefore, the etch starts from the top of the formed nanoposts and pills off the tapered part until a steady state is achieved where a hexagonal nanowire is formed with C-plane and M-plane facets. Fig. 3.5(c) and (f) illustrate the obtained nanowires with uniform surface and straight sidewalls. Experimentally, a two-hour etch duration is needed to reach the state. Note that the etch process does not stops when the tapered part of the posts are removed, but rather it shrinks the nanowires at a relatively lower etch rate. This offers us the ability to control the nanowire diameter by managing the wet etch duration.

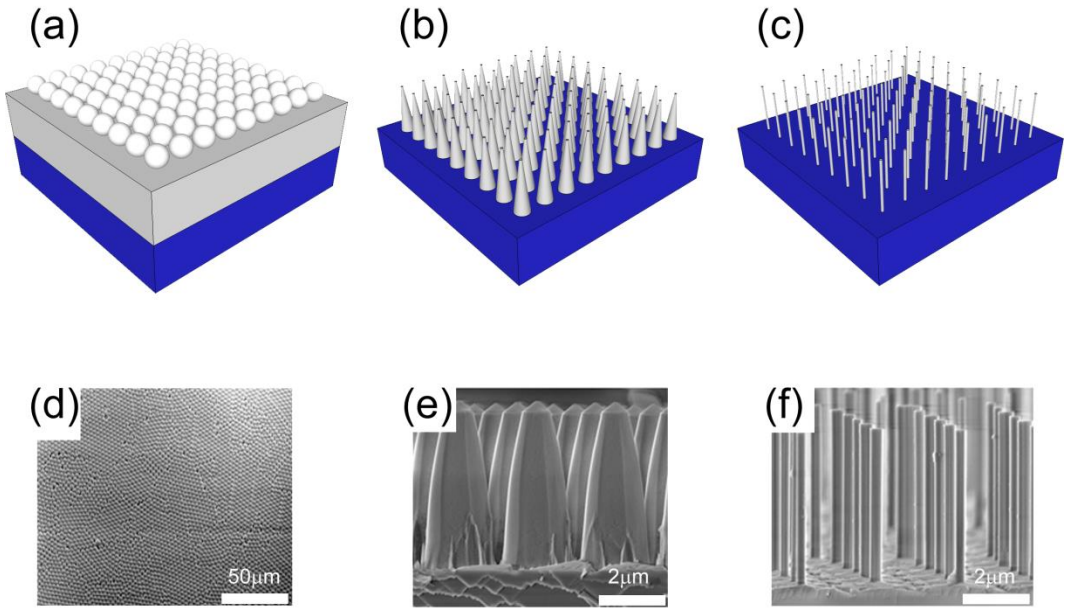

Figure 3.5 Schematic of nanowire fabrication process by means of the two-step top-down etch technique. (a) sphere coating on the GaN substrate; (b) taper-shaped nanoposts formed after the ICP dry etch; (c) nanowire formation after a anisotropic wet etch process; (d)-(f) show the SEM images of fabrication steps corresponding to (a)-(c) respectively.

It is also feasible to produce arbitrary shaped GaN nanodevices by combining the electron beam lithography and the top down techniques. Fig. 3.6. illustrates the procedure to fabricate nanostructures using this approach. Fig. 3.6(a) sketches a metal ring mask defined on a thin-film GaN substrate by the electron beam lithography. After the ICP dry etch, the ring structure is transferred to the GaN film with tapered and ununiformed sidewalls (Fig. 3.6(b)). The following AZ400K wet etch removes the damages from the dry etch process and generates straight and smooth sidewalls (Fig. 3.6(c)). Fig. 3.6(d)-(g) also show the SEM images of various structures fabricated by this technique, including nanorings, “figure-8” resonators, and nanospirals.

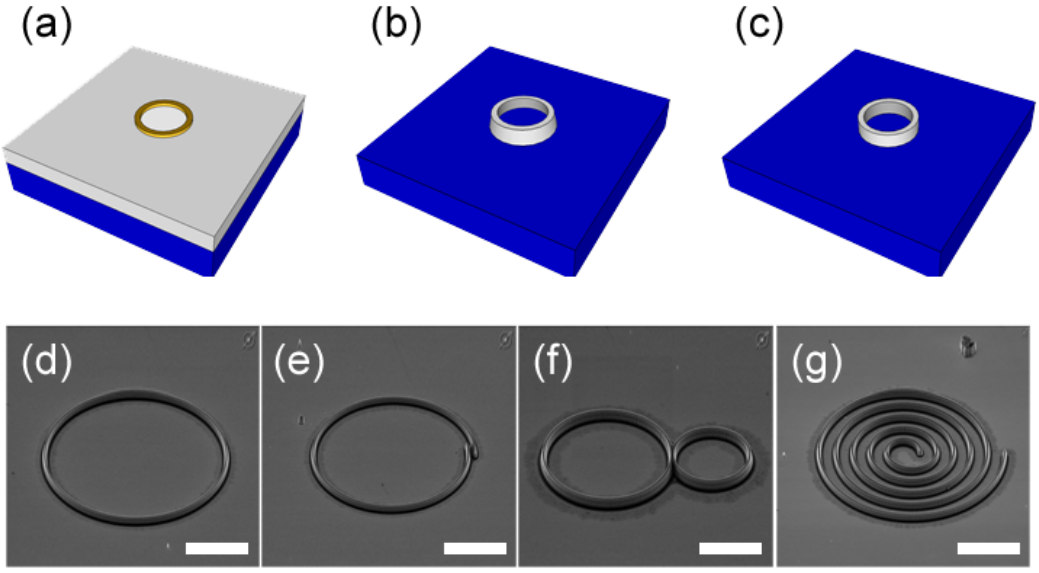

Figure 3.6 Schematic of arbitrary nanostructure fabrication process by the e-beam lithography plus the top-down etch techniques. (a) metal coating on the GaN substrate by the electron beam lithography; (b) taper-shaped nanoring formed after the ICP dry etch; (c) nanoring formation after a anisotropic wet etch process; (d)-(g) show the SEM images several nanostructures fabricated by this technique. The scale bars represent 1 μm.

3.1.3 Issues about the top-down technique

While the top-down etch approach shows the capability of fabricating various GaN nanostructures, it is challenging to produce III-nitride devices with different material components. This is due to the reason that the wet etch rate varies with different III-nitride materials so that smooth sidewalls of the structures are hardly be obtained. The roughness of the structure surface will strongly enhance the surface scattering effect, leading to the low optical performance of these nanostructures.

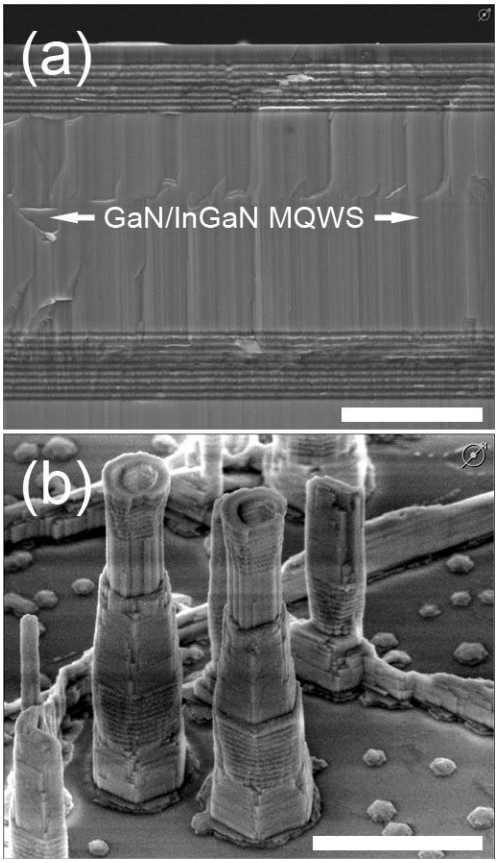

Figure 3.7 SEM images of (a) cross-sectional view of cleaved III-nitride epilayer with two DBRs respectively composed of 8 and 10 periods of AlN/GaN stacks and 5 periods of GaN/InGaN multiple quantum wells; (b) formed nanoposts after the top-down etch process. The scale bars represents 3 μm.

An example of this issue is illustrated in Fig. 3.7, where nanoposts are fabricated from a III-nitride thin film with different III-nitride materials. Fig. 3.7(a) shows a cross-sectional SEM image of the thin film. ~4 μm GaN layer is sandwiched by two (top and bottom) distributed Bragg reflectors (DBRs), with the top DBR consisted of 8 periods and the bottom consisted of 10 periods of AlN/GaN stack layers respectively. In the middle of the GaN layer, 5 periods of GaN/InGaN multiple quantum wells (MQWs) is grown as the gain media. The top-down etch technique is expected to produce nanowires

with the DBRs and the MQWs for the purpose of generating visible nanolasers with low lasing threshold. After the top-down etch, the resulting nanoposts are shown in Fig. 3.7(b). It is seen that the sidewalls of the nanoposts are ununiformed with clear steps observed at the interfaces between different materials. In addition, a etch rate difference of InGaN > GaN > AlN is also observed. This effect makes it challenging to generate high quality III-nitride nanodevices with more than one material components directly from the top-down etch.

3.2 Optical characterization of the nanowires

This section introduces the techniques used to characterize the optical properties of the GaN nanowires. Micro-photoluminescence (μ-PL) setup is described which is commonly used to characterize the emission spectrum of the nanowires. Moreover, we also developed a dual-arm μ-PL system, which has a separate collecting arm oriented perpendicular to the pumping arm. This technique allow us to characterize the emission power, polarization and far field energy distribution of the laser emission from the nanowires.

3.2.1 Micro-photoluminescence setup

The optical properties of the nanowires are characterized using a μ-PL setup, as shown in Fig. 3.8. The pump laser used is a frequency-quadrupled Nd:YAG laser operating at 266 nm with a pulse duration of 400 ps and a repetition rate of 10 kHz. The output power of the pump laser is ~10 mW. A set of spatial filter is employed to enhance the beam quality of the pump light, after which the light power reduces to ~1 mW. A set of neutral density

filters is used for the further controlled reduction of the pump power. The nanowire is excited using the pulsed laser through a 50× ultraviolet objective with a 5 μm spot size, and the emission from the nanowire is collected by the same objective and analyzed using a CCD detector and a 300 mm spectrometer with a 1200 or 2400 groove/mm holographic grating. Note that the pump spot size can be changed by using another set of spatial filter, which gives a ~1 μm exiting spot.

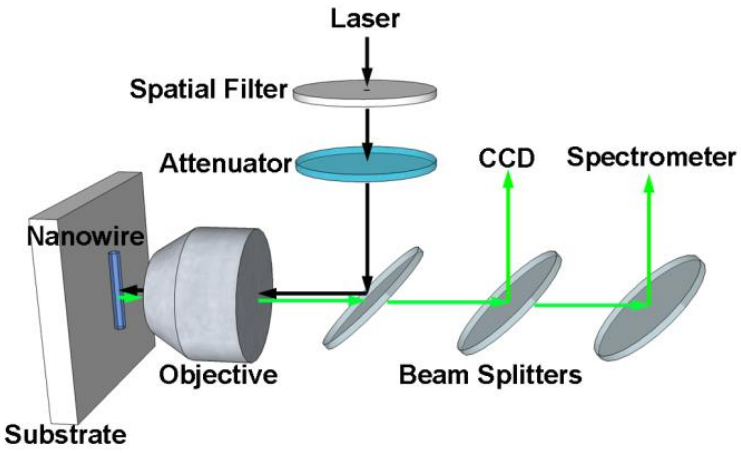

Figure 3.8 Sketch of experimental setup for nanowire excitation and micro-photoluminescence measurement.

3.2.2 Dual-arm micro-photoluminescence setup

In addition to the commonly used μ–PL setup introduced above (one-arm μ–PL setup), we develop a dual-arm μ–PL setup for analyzing the light emission directly from the nanowire end-facets. Different with the one-arm μ–PL setup in which the pumping objective functions as well for the light collection, the dual-arm setup employs another arm to collect and analyze the emitted light. As illustrated in Fig. 3.9, the second arm (collecting arm) involves a 20X ultra-violet objective, a polarizer, and a Charge-coupled

device (CCD) detector or a 300 mm spectrometer with a 1200 or 2400 groove/mm holographic grating. The collection arm is orientated perpendicular to the pump arm so that the nanowires can be pumped from the side and at the same time their emission can be collected directly from the end facets. There are three main advantages of the dual-arm setup for the light characterization. Firstly, the direct analysis from the end-facet emission allows for measuring the far-field distribution that is hard to achieved in a one-arm setup which collects light from an orientation perpendicular to the nanowire emission direction. In addition, the lasing power can be measured precisely since only a large fraction of the emitted light can be captured from the on-axis direction. Moreover, by using the dual-arm setup, substrate scattering effect on depolarizing the emission can be intensely alleviated, which allowing for precise analysis of the light polarization.

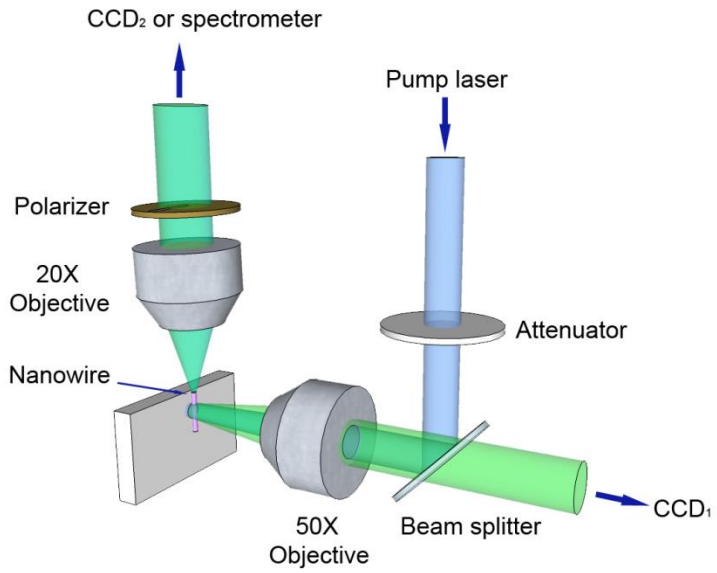

Figure 3.9 Sketch of dual-arm micro-photoluminescence setup used for analyzing the light emission directly from the nanowire end-facets.

3.3 Simulation techniques for the nanodevices

The nanodevices properties are analyzed using a FDTD technique. The FDTD is a numerical analysis technique that can be used for finding approximate solution of Maxwell equations.[63] The FDTD technique is a time-domain method, whose solution can cover a wide frequency range and treat nonlinear material properties with a single simulation run. The FDTD is numerical modeling method which belongs in the grid-based differential time-domain methods. The partially-differential time-dependent Maxwell's equations are discretized to the space and time partial derivatives using central-difference approximations. The resulting finite-difference equations are solved in a leapfrog manner: the electric field vector components in a volume of space are solved at a given instant in time; then the magnetic field vector components in the same spatial volume are solved at the next instant in time; and the process is repeated over and over again until the desired transient or steady-state electromagnetic field behavior is fully evolved.

A commercial package from Lumerical Inc is utilized to solve the finite-difference equations. The nanowire passive cavity eigenmodes are determined using a fully vectorial commercial Mode Solver from Lumerical Inc, which is a comprehensive waveguide design environment for designing, analyzing and optimizing components made from waveguide structures, including planar integrated optical waveguides and optical fibers.[63] Mode solutions include both an eigenmode solver for waveguide and fiber modal analysis, as well as a 2.5D FDTD propagation method for analyzing how optical fields propagate within waveguiding structures. While typical applications include the design of planar waveguide layer structures, passive waveguide components, and

microstructured optical fibers, MODE Solutions can also address nonlinear effects and waveguide-based amplification.

Chapter 4

Single-Mode Lasing in GaN Nanowire-Pairs

Semiconductor nanowire lasers have sparked tremendous scientific and technological interest as potential ultracompact and low power consumption nanolasers.[18,28,64] The properties of these nanowires, such as compact cavity structure and sub-wavelength waveguide, offer novel interesting lasing features and promise in constructing nanoscale photonic and optoelectronic circuits and devices[65,66]. For many practical applications, such as imaging, multiplex communication, and data storage, nanowire lasers are required to have high spectrum purity and beam quality so that desired functionality, such as resolution, can be achieved. These conditions can be satisfied if single-mode operation is achievable in nanowire lasers. Therefore, development of nanowire lasers with single-mode operation is critical for realizing these practical applications.

However, due to the lack of mode selection mechanisms, most reported nanowire lasers exhibit multimode behavior[18,67]. Single-mode, as-fabricated Fabry-Perot GaN nanowire lasers have been demonstrated by precise control of the nanowire geometry (diameter and length) to reduce the number of transverse and longitudinal modes[32]. However, this approach limits the GaN nanowire diameter to < ~130 nm and length to < ~ 5 μm, which could limit nanolaser design flexibility and reduce cavity gain, and could also potentially increase surface-related defects and surface depletion effects from the higher surface-to-volume ratio[68]. Another way of addressing this issue is to make use of

coupled cavities[33,46,55], which can generate a mode selection mechanism by the Vernier effect. This technique has been employed to realized single-mode lasing from CdSe nanowires, where "8"-shaped and "X"-shaped cavities were introduced to ensure the coupling. In these nanowire lasers, the lasing wavelength (738 nm) is much larger than the nanowire diameter (200 nm[46] and 420 nm[55]) so that the nanowires, without the coupled cavities, is believed to support a single transverse and multiple longitudinal modes. However, it is more complicate to achieved single-mode lasing in nanowires with diameter comparable or even larger than emission wavelength, where both multiple longitudinal and transverse modes need to be suppressed to achieve single-mode lasing.

Since the GaN nanowire lasers operate at ~370 nm, comparable to the nanowire diameter, the mechanism of multiple transverse mode suppression, as well as that of multiple longitudinal mode, needs to introduced to achieve single-mode lasing. This chapter will introduce stable single-mode lasing operation from a pair of coupled GaN nanowires. The GaN nanowires with different length are placed side-by-side in contact to form a coupled cavity through nanoprobe manipulation. Unlike individual nanowire lasers, which operate in a combined multi-transverse and multi-longitudinal mode oscillation, a coupled nanowire provides a mode selection mechanism through Vernier effect, which can strongly enhance the free spectrum range between adjacent resonant-modes and generate a stable single-mode operation with a high side mode suppression ratio. This result for the first time demonstrates the full potential of Vernier effect for simultaneous suppression of both multiple transverse and longitudinal mode in coupled GaN nanowire cavities.

4.1 Experimental results

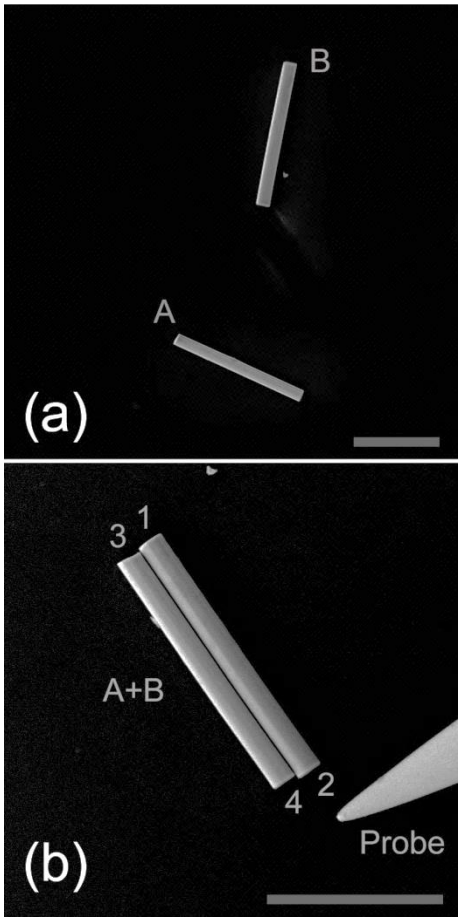

Figure 4.1(a) Individual GaN nanowires. The scale bar represents 10 microns. (b) The GaN nanowires was manipulated into a coupled nanowire cavity. The scale bar represents 5 microns.

The GaN nanowires are fabricated by means of the two-step top-down etch technique, as described in chapter 3. For optical characterization, the nanowires are transferred to Si substrates covered with a 100 nm thick silicon nitride (Si_3N_4) thin film. The optical properties of the individual nanowires are studied using the one-arm micro-photoluminescence (PL) setup as detailed in chapter 3. Note that this setup can achieve a

~5 μm or ~1 μm pump spot size with a two different single sets of spatial filters. To obtain a uniform illumination on the nanowires, the ~5 μm spot is commonly employed for the optical pumping. Since the nanowires used in this experiment is ~8 μm in length, we illuminate the center region of the nanowires. Following measurements on individual nanowires, the same nanowires are manipulated into coupled cavities using a piezo-electric nanoprobe inside a scanning electron microscope (SEM) and measured with the same technique.

Fig. 4.1(a) shows a SEM image of two individual nanowires A and B with diameter/length of 680 nm/7.6 μm and 720 nm/8.0 μm, respectively. A typical PL spectrum pumped below threshold (from nanowire A) is shown in Fig. 4.2(a). It is seen that the spectrum covers a range of ~20 nm with a full width at half maximum (FWHM) of 7.4 nm. At this low pump level, the CCD image shows roughly uniform optical emission from the entire nanowire length, indicating that unguided (out-of-plane) and guided (on-axis) emission intensities are basically equal (see Fig. 4.3(a)). The inference is that the optical emission is entirely from spontaneous emission. When pumped above lasing threshold, the individual nanowires display many salient features evidencing lasing behavior. The first feature is that a distinctly different emission pattern emerges in the CCD image. The on-axis emission grows significantly, appearing as two bright spots at the ends of the nanowire indicative of Fabry-Perot lasing, as shown in Fig. 4.3(b).[32] The light collected by the objective lens is directly from the highly diverging output beam and indirectly from scattering of the output beam by the SiN surface. The large divergence angle of output beam is because of diffraction from a sub-wavelength nanowire aperture. At the same time, there is a clamping of the unguided spontaneous emission, which

appears as a darkening (relative to the bright ends and with filters in place) of the entire length of the nanowire, also shown in Fig. 4.3 (b). Also present in the CCD image are concentric rings of optical interference fringes, which is an indication of the spectral coherence of the emitted light, indicating the lasing behavior of the nanowire. The second feature is the sudden appearance of sharp spectral peaks from the spectrometer, with a bandwidth of ~0.14 nm for each peak, as shown in Fig. 4.2(b) (red curve).

The lasing behavior of the individual GaN nanowires shows multiple transverse/longitudinal modes. This feature is evidenced by the uneven spacing between the lasing peaks. For a nanowire to function as a single-mode waveguide, the nanowire geometry should satisfy $(\pi D/\lambda)\left(n_1^2-n_0^2\right)^{0.5}<2.405$ [16], where D is the nanowire diameter, λ is the wavelength in vacuum, and n_1 and n_0 are the refractive indices of the nanowire and the surrounding air, respectively. From this equation, we calculated the critical diameter to be ~130 nm for a GaN nanowire to function as a single transverse-mode waveguide. Therefore, for a GaN nanowire with a diameter of ~700 nm, the lasing will be dominated by multi-transverse modes. For each transverse mode, a set of longitude modes is activated with the free spectral range (FSR) determined by $\Delta\lambda_{FSR}=\lambda^2/2n_gL$, with λ, L, n_g representing wavelength in vacuum, cavity length, and group refractive index, respectively. Therefore, multiple transverse modes give rise to multiple sets of longitude modes with different FSRs, because n_g varies with different transverse modes. The overlapping of all sets of longitude modes leads to an uneven spectral map for possible lasing wavelengths. In addition, mode competition[69] and the spatial hole-burning effect[70] selectively support certain modes and shape the uneven-spaced lasing spectrum. We note that the spectral spacing shown in Fig. 4.2(b) is much smaller than the predicted

FSR of ~1.53 nm for a single transverse-mode operation (using n_g=5.6[71], *D=370* nm and *L=8* μm for the calculation), which further verifies the multiple transverse-mode operation of the laser.

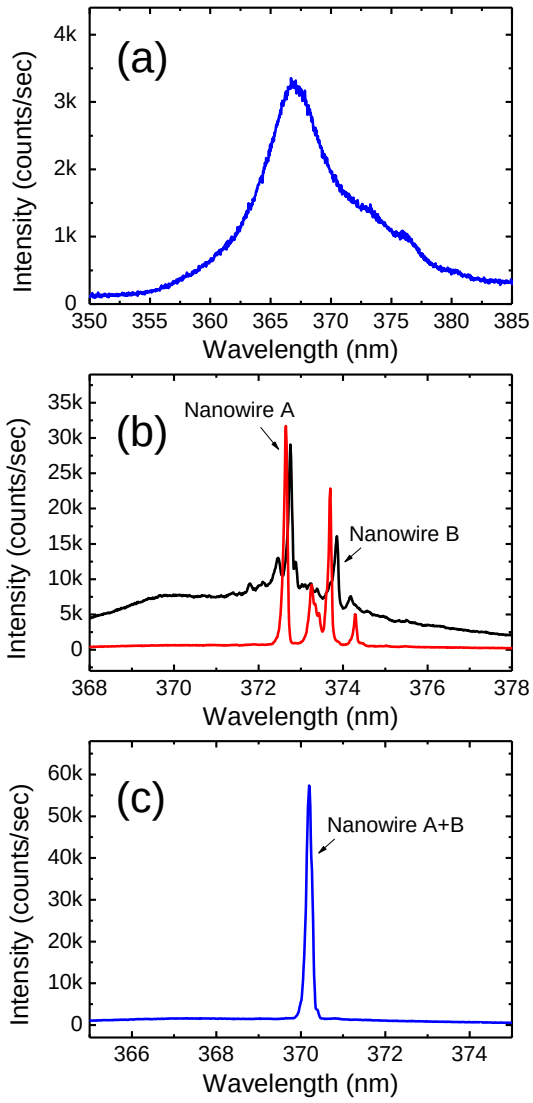

Figure 4.2 Lasing emission spectra of the coupled nanowire pair and corresponding separated individual nanowires. (a) a spontaneous emission spectrum obtained from nanowire A; (b) lasing spectra from individual nanowire A and B respectively; (c) lasing spectrum obtained from the nanowire pair. (b) and (c) are obtained with the same pump intensity of 1429 kW/cm^2.

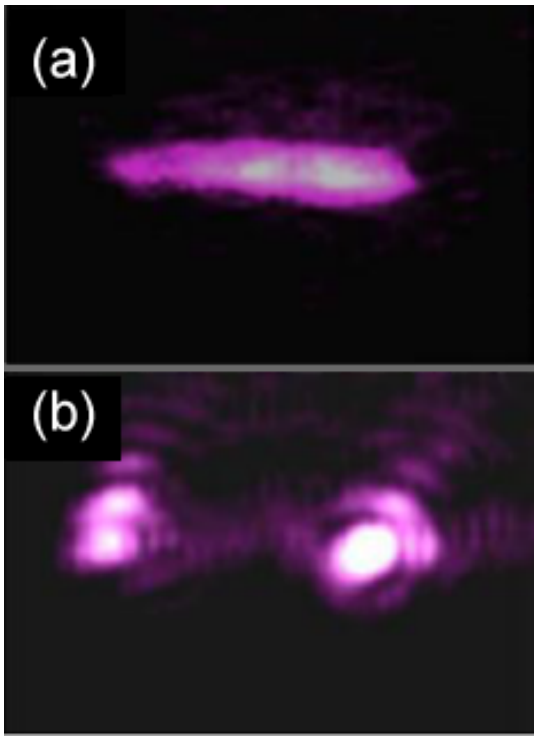

Figure 4.3 (a) and (b) are CCD images of a GaN nanowire pumped below and above lasing threshold, respectively. The nanowire laser emits a highly divergent beam from the facets, some of which is collected by the objective lens. The objective lens also collects radiation emitted from the facets that is scattered by the SiN substrate surface, as well as spontaneous emission exiting perpendicular to the nanowire axis. (figure taken from [32])

The coupled cavity formed by these two nanowires is shown in Fig. 4.1(b). Below lasing threshold, the PL emission from the nanowire pair was similar to that of an individual nanowire, showing a wide-band spectrum. However, above threshold, the nanowire pair exhibited single-mode lasing properties. As the pump intensity increased to 874 kW/cm^2, a single sharp peak emerged from the wide-band PL background. Further increase of the pump intensity led to a corresponding increase of the spectral peak and a larger signal-to-noise ratio. Fig. 4.2(c) shows a typical spectrum of the single-wavelength

lasing at a pump intensity of 1429 kW/cm^2. It is seen that the lasing peak is located at 370 nm with a side mode suppression ratio (SMSR) of ~15.6 dB. Lorentzian fitting of the spectrum gives a FWHM of ~0.14 nm. The lasing is stable with no spectral mode-hoping observed during the experiment. The lasing threshold of the nanowire-pair measured is 874 kW/cm^2, which is comparable for that of each individual nanowire.

4.2 Discussions

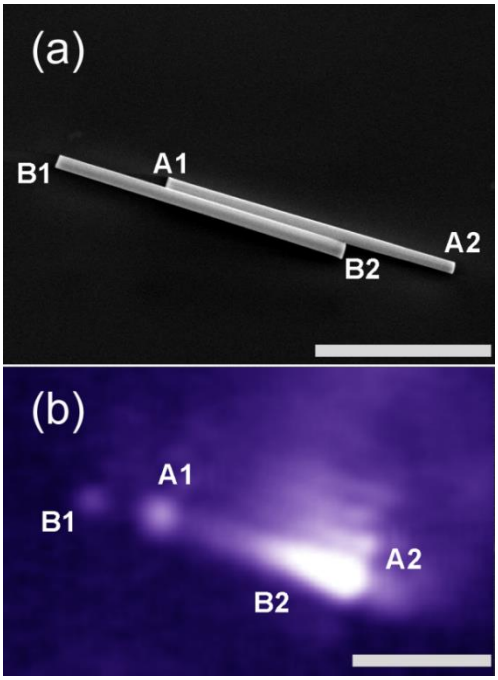

Figure 4.4 (a) SEM image of partial overlapped two nanowires for verifying the evanescent coupling; (b) the obtained CCD image when the A2 end of nanowire A is optically pumped. The scale bars represent a length of 3 μm.

The simultaneous suppression of both multiple transverse and longitudinal mode operation for the coupled nanowires originates from a mode selection mechanism enabled by evanescent interaction between the two nanowires. Energy transfer through

evanescent coupling is demonstrated[72] and modeled[73] for closely located nanowires. To verify the coupling effect in our nanowire-pairs, we short the overlapping length of two nanowires, and then selectively pump one nanowire and observe the emission from the other one. To prevent the two nanowires from being pumped simultaneously, the spatial filter with a pump spot of ~1 μm is utilized. As shown in Fig. 4.4(a), when one end of nanowire A2 is pumped, the emission is observed from the bottom end of B2, as evidenced by the CCD image shown in Fig. 4.4(b). This result evidences that the light is able to transfer between the two nanowires, verifying the effective coupling effect. This coupling effect transforms a nanowire pair into a coupled cavity. In this coupled cavity, a set of resonance conditions has to be satisfied, i.e. simultaneous oscillation of each sub-cavity.[74,75] In the nanowire pair cavity shown in Fig. 4.1(b), the new resonance condition is the simultaneous oscillation of four sub-cavities of *12*, *14*, *23*, and *34*. Since $L_{12}+L_{34}=L_{14}+L_{23}$ and $L_{13}=L_{24}$, the resonance condition will be simplified to the simultaneous oscillation of sub-cavity *12* and *14*.

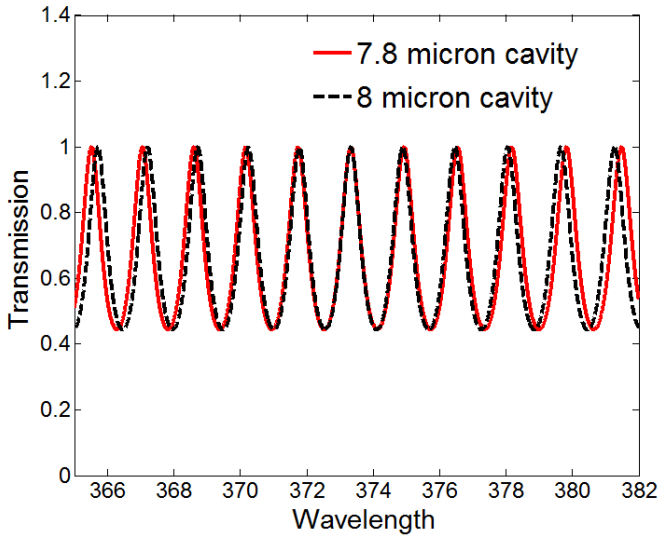

Figure 4.5 Calculated transmission of the 7.8 and 8 μm cavities.

Since the diameters of the GaN nanowires are much larger than their emission wavelengths, in each sub-cavity many transverse modes exist with different value of group refractive index (n_g) ranging from 5.0 to 6.0[71]. For each of these transverse modes, the longitudinal modes can be expressed using

$$T(\lambda) = (1-R)^2 / \left[(1-R)^2 + 4R\sin^2(2\pi L n_g / \lambda) \right],$$

where T is the transmission of cavity, L is the nanowire length, n_g is the group refractive index, and R is the reflectivity at each nanowire facet ($R = (n - n_0 / n + n_0)^2 \approx 0.2$ when refractive index $n=2.6$[71]). From this equation, the resonant wavelengths of longitude modes for each sub-cavity can be calculated. These resonant wavelengths are compared to determine overlapping resonant wavelengths between sub-cavity *12* (8 μm cavity) and *14* (7.8 μm cavity) as shown in Fig. 4.5. It is seen that the modes of these two sub-cavities overlaps at ~373.3 nm and start to deviate from each other when the wavelength is shifted. Moreover, this calculation reveals that the spectral range of two overlapping wavelengths of the coupled nanowire cavity is about 50 nm, much larger than the gain bandwidth. Therefore, the overlapping mode at 373 nm is likely the only possible lasing mode for the coupled cavity. Note that this calculation assume a transverse mode with $n_g=5.6$. As n_g varies with different transverse modes, the overlapping mode may shift away from the gain range (approximately GaN emission range) and not oscillate. In other words, only the transverse mode with proper n_g can be selected by the coupled nanowire cavity. Fig. 4.6 shows the calculated resonant wavelengths of the coupled cavity as n_g varies from 5.0 to 6.0. For each n_g, three overlapping resonant wavelengths near the gain are plotted in the figure. It is seen that there exists a resonant wavelength located within

the gain band only when n_g is in the range from 5.47 to 5.64. Therefore, the coupled nanowire cavity provides a mechanism for selecting a transverse mode and thus functions as a single transverse mode laser.

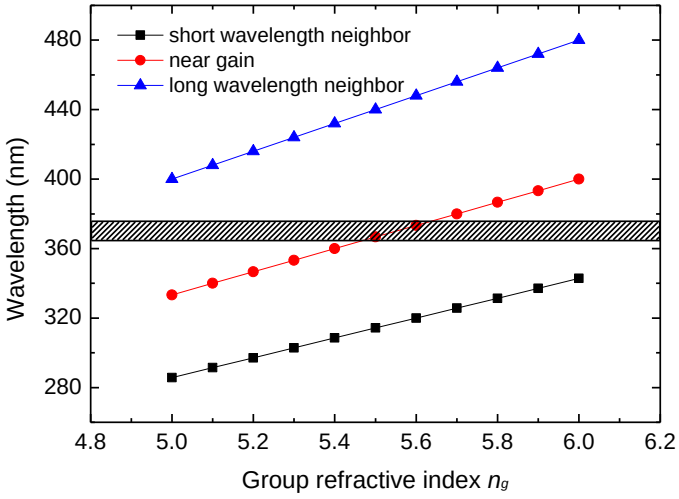

Figure 4.6 Overlapping wavelengths for the nanowire-pair versus effective group refractive index n_g. Three points nearest the gain spectrum are plot for each n_g. The shaded area indicates the gain bandwidth.

4.3 Summary

In this chapter, we introduced the demonstration of a single-mode GaN nanowire laser by placing two nanowires side-by-side in contact to form a nanowire-pair. The nanowire-pair lases at 370 nm with a threshold of 874 kW/cm^2 and a SMSR of 15.6 dB is observed. The mode selection of the nanolaser is achieved by the Vernier effect, which in this letter is shown to suppress the multiple transverse mode oscillation as well as multiple longitude mode oscillation of the GaN nanowires. The results indicate a promising approach for transverse-mode selection in nanowires where the nanowire diameter is much larger than the wavelength.

Chapter 5

Gold-Substrate Induced Single-Mode Lasing in Individual GaN Nanowires

As presented in Chapter 4, by placing two GaN nanowires side-by-side in contact, single-mode lasing can be generated. This technique opens insight to realize single-mode lasing in short-wavelength emission nanowires with comparable large nanowire diameters. However, this technique relies on the nano-manipulation to form the coupled cavities, which makes the process complicated. In this chapter, we introduce an alternative technique to realize single-mode nanowire lasers by contacting a GaN nanowire, which otherwise exhibits multimode lasing properties, to a gold substrate. The difference in the spatial distribution of different transverse modes causes them to be attenuated differently by the presence of the metal. This is confirmed by a FDTD simulation result, which demonstrates that high-order transverse modes have much larger attenuation compared with the fundamental mode. Therefore, the nanowire-gold contact generates a mode-dependent loss, which can strongly attenuate higher guiding modes and ensure the single transverse mode operation. One-dimensional length control of the nanowires is utilized for multiple longitudinal-mode suppression.[32] Using this technique single-mode emission at ~369 nm of a ~350 nm diameter nanowire is demonstrated with a side-mode suppression rate of 17.4 dB and a bandwidth of 0.12 nm. These results provide guidance

for the design of nanolasers and offer a practical method of realizing single-mode nanoscale light-emitting devices.

5.1 Transverse mode selection by a lossy substrate

GaN nanowire lasers typically exhibit multiple transverse-mode and multiple longitudinal-mode oscillation.[33] In order to obtain single-mode operation, it is necessary to introduce a multimode suppression technique to the nanowire cavity. Previously, we have demonstrated that multiple longitudinal-mode oscillation in GaN nanowires can be suppressed by reducing the nanowire length to ~5 μm, at which point the mode competition is strongly enhanced in the cavity.[32] Here, we concentrate our efforts on the issue of multiple transverse-mode suppression. Single transverse-mode GaN nanowire lasers have been demonstrated, but this approach requires diameters below a critical diameter of ~130 nm.[32] Transverse-mode selection techniques in macroscopic lasers, such as placing an intra-cavity pinhole into a bulk laser cavity[76,77], have been widely studied. In principle, this technique could work for nanowire lasers but would be difficult to achieve due to the small cavity volume and potential material damage from lithographic or electron and ion-beam nanostructuring methods. Alternatively, the light field inside a nanowire waveguide can be manipulated by affecting the evanescent wave of the waveguide modes, so as to generate an attenuation effect.[78, 79] Here, we propose a transverse-mode selection technique by means of an absorptive material serving as the nanowire substrate. Due to moderate ohmic loss in the ultraviolet band, gold is selected as a substrate material for achieving a single-mode GaN nanolaser. Note that this proposed on-metal dielectric nanolaser differs from the recently reported plasmonic

nanolasers that rely on metallic guided modes. In the case of the plasmonic laser the electric field is highly confined by the metallic structure.[80, 81, 82] This contrasts from our proposed nanolaser since the mode is guided in the dielectric and the metal acts purely as a loss mechanism for high-order modes. Moreover, due to the difference in the spatial distributions, the cavity loss varies with different transverse modes, thereby generating the mode-dependent loss.

5.2 Simulation results

To investigate the proposed mode-dependent loss mechanism, we first conduct simulations to illustrate the modal properties of GaN nanowires placed on a gold substrate. The nanowire passive cavity eigenmodes are determined using a fully vectorial commercial mode solver from Lumerical Inc, which is widely used to analyze mode distribution, frequency response, and propagation loss of nanoscale waveguides.[63] In this simulation, a cylindrical nanowire is defined on top of a gold substrate (200 nm thick). The operation wavelength is set as 370 nm (near the GaN bandedge emission wavelength). The refractive index of GaN is assumed to be 2.6[71], and the real part and imaginary part of gold are set as 1.70 and 1.88 respectively[83] (these values correspond to a wavelength of ~370 nm). The transverse modes supported by this geometry are analyzed by a two-dimensional cross section calculation in a $1\,\mu m \times 1\,\mu m$ window (perfectly matched layer boundary conditions are used), where 200 unit cells in both x and y directions are employed to ensure the simulation accuracy. The dimensions of the nanowires can be modified to study the substrate effect on nanowires with different geometry.

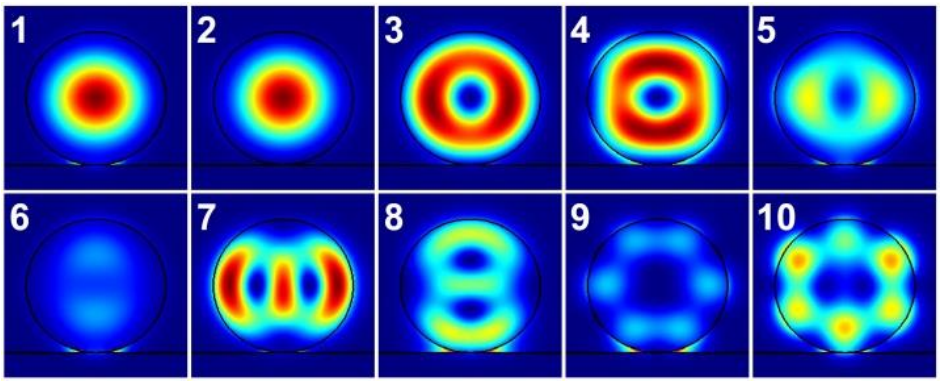

Figure 5.1 Transverse modes supported by the nanowire-metal geometry. The black circle and straight line indicate the surfaces of the nanowire and metal substrate, respectively.

	Mode 1	**Mode 2**	**Mode 3**	**Mode 4**	**Mode 5**
Loss (dB/cm)	8151	1730	4806	7109	16041
	Mode 6	**Mode 7**	**Mode 8**	**Mode 9**	**Mode 10**
Loss (dB/cm)	34858	7551	22205	29175	28706

Table 5.1 Propagation loss for the different modes supported by a 300 nm diameter nanowire (operation wavelength: 370 nm).

Fig. 5.1 shows the transverse mode distributions supported by a 300 nm diameter nanowire placed on the gold substrate. It is seen that ten modes are supported by this geometry. Due to the presence of the metal substrate, the mode degeneracy is broken, with modes in each order showing different polarization, mode distribution, and propagation loss (no propagation loss obtained from similar simulations of nanowires

with a dielectric substrate). Table 5.1 shows the propagation loss for the different modes, showing that the propagation loss is sensitive to mode distribution, i.e., more absorption occurs for modes that have more of their modal fraction confined within the metal region. Mode 2 has the smallest propagation loss of 1730 dB/cm (corresponding to an extra 1.83 dB or 34.4 percent cavity loss for a 5.3 μm nanowire cavity), which is significant lower than that of the other modes. Mode 3 has the second smallest loss of 4806 dB/cm, corresponding to an extra 5.09 dB or 84.7 percent cavity loss for a 5.3 μm nanowire cavity. Therefore, single transverse-mode lasing is expected since Mode 2 will be the only mode with a cavity loss that is attainable by the modal gain. Further simulations are also conducted for nanowires with different diameters, and it is found that higher/lower losses will be generated with reduced/larger nanowire diameters. Regardless, in all cases, a mode-dependent loss can be always obtained. With further simulations, we find that nanowires with diameters ranging from ~250 to ~400 nm are suitable for generating single transverse-mode operation since one specific mode experiences much less attenuation than the others.

5.3 Experimental results

GaN nanowires with the expected proper geometry for single-mode lasing operation are then fabricated and optically characterized to experimentally verify the modeling results. The GaN nanowires are fabricated by a top-down, two-step etch technique, detailed in Chapter 3. This technique is able to produce vertically aligned c-axis oriented nanowires with precisely controlled geometries from c-plane GaN epilayers, and the fabricated nanowires have straight and smooth sidewalls. Here, nanowires are intentionally

fabricated with ~300 nm diameter and ~5.3 μm length for the purposes of verifying the simulation results and bypassing the multiple longitudinal-mode oscillation[32], respectively. These nanowires are then transferred to a Si_3N_4 (300 nm thick) on silicon substrate photolithographically patterned with gold regions (200 nm thick and 120 μm diameter) for optical characterization. The structure of the substrate is sketched in Fig. 5.2. The optical properties of the nanowires are characterized using the one-arm micro-photoluminescence setup, as described in Chapter 3.

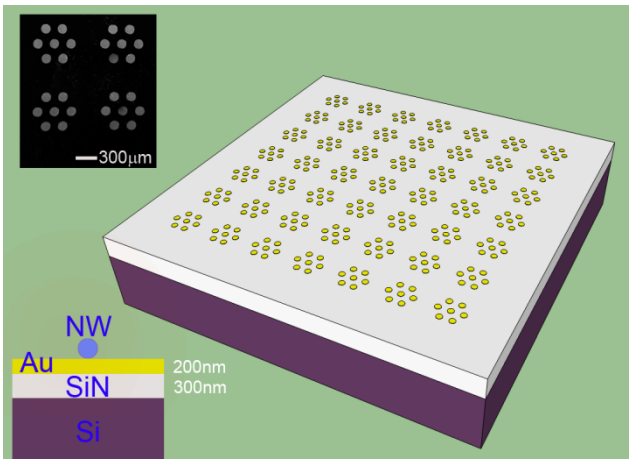

Figure 5.2 Schematic showing the Si_3N_4 film selectively patterned with gold spots for optical characterization of the GaN nanowires. The inset shows an SEM image of the gold spots.

As a baseline, the lasing properties of GaN nanowires on areas of the Si_3N_4 film (without gold) are first investigated. Then, in order to examine the impact of the gold substrate on the lasing properties, these same nanowires are subsequently transferred onto a gold-coated area of the membrane with a piezo-electric driven tungsten probe. Fig. 5.3(a) shows a scanning electron microscope (SEM) image of a GaN nanowire ~350 nm in diameter and ~5.3 μm in length lying on the Si_3N_4 film.

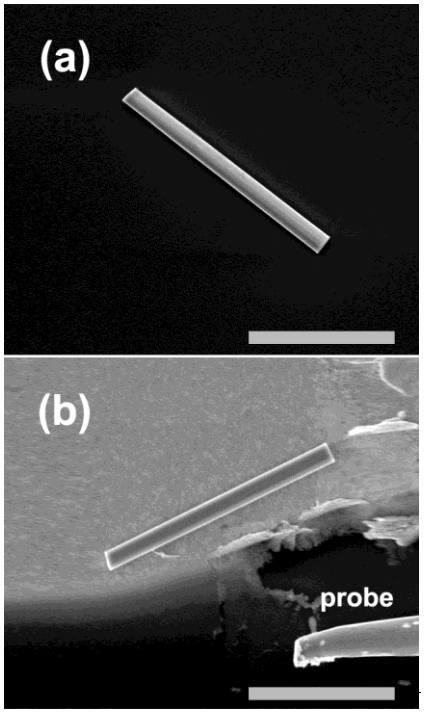

Figure 5.3 SEM images of the same GaN nanowire (a) on top of the Si_3N_4 film; and (b) after being transferred onto a gold-coated region. The scale bars represent 3 μm.

Below threshold, the nanowire shows a broadband photoluminescence (PL) emission, with a spectrum centered at 367.5 nm and a full-width half-maximum of ~7.5 nm. Lasing is observed by gradually increasing the pump power with a threshold of 241 kW/cm^2. Fig. 5.4(a) shows typical lasing spectra at different pump powers. The blue curve shows the measured spectrum when the nanowire is pumped slightly below threshold, with several small peaks apparent. Upon increasing the pumping intensity beyond threshold, most of these peaks grow with an enhanced signal-to-noise ratio; moreover, new resonant peaks also emerge, as shown in the red spectral curve (276 kW/cm^2). The black curve shows the spectrum at a pump power of 458 kW/cm^2. Six primary peaks are seen in the spectrum with an uneven spectral spacing. A minimum spacing of ~0.58 nm is observed, much smaller than the calculated longitudinal mode

spacing of ~2.1 nm for single transverse-mode operation.[33] Taken together, these spectral features are indicative of multiple transverse-mode operation of the GaN nanowire laser.[33]

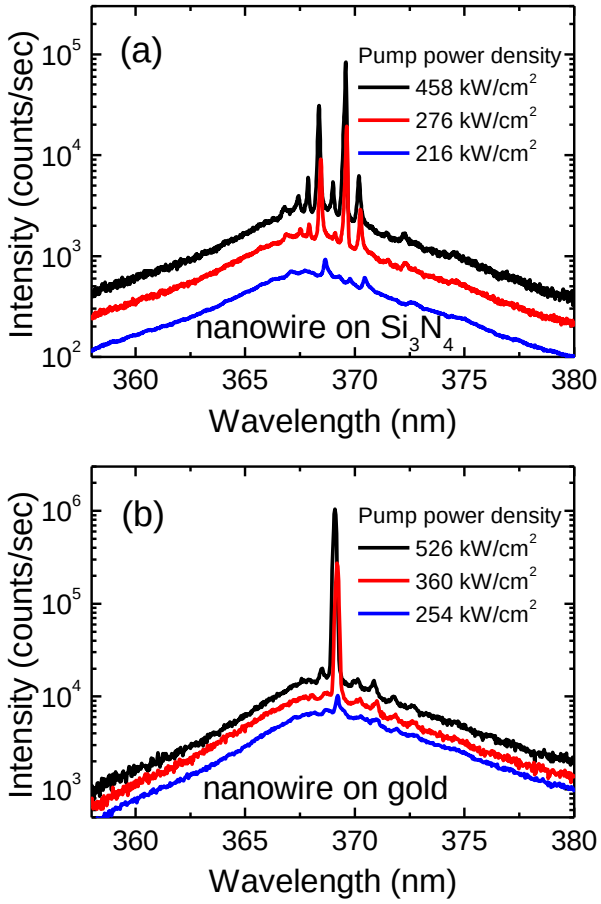

Figure 5.4 Spectra of a GaN nanowire lasing (a) on Si_3N_4 and (b) after being transferred onto gold.

Fig. 5.3(b) shows the SEM image of the same nanowire after its transfer onto a gold-coated region of the substrate. Under gradually increased optical pumping, a similar spectral evolution from PL to lasing is observed, as seen in Fig. 5.4(b). Due to the extra cavity loss introduced by the metal substrate, the observed lasing threshold increases to 276 kW/cm^2, ~13% larger than that observed directly on the Si_3N_4 substrate. However,

when pumped above threshold the nanowire placed on gold exhibits single-mode lasing behavior, distinctly different from the multimode lasing observed for the same nanowire on Si_3N_4. The blue curve in Fig. 5.4(b) shows the emission of the nanowire when pumped slightly below threshold, exhibiting only one dominant peak at 369.3 nm. This remains the case as the pump power increases above threshold (red and black curves). Under a pump intensity of 526 kW/cm^2, well above threshold, single-mode lasing with a side-mode suppression ratio (SMSR) of 17.4 dB and a bandwidth of 0.12 nm, the resolution limit of the spectrometer, is measured (via Lorentzian fitting). In order to further confirm this effect, the experiment is repeated with different nanowires whose diameters ranged from ~250 to 400 nm. A similar transition from multimode to single-mode lasing operation is also observed when these nanowires are transferred from the Si_3N_4 to the gold-covered regions. Thus, the predicted mode-sensitive loss mechanism induced by placement of the nanowire on the gold surface is confirmed.

5.4 Summary

In this chapter, we demonstrate a new mechanism for lasing-mode selection by coupling a GaN nanowire laser to an underlying gold substrate. A mode-dependent loss can be induced by the gold substrate to suppress multiple transverse-mode operation and thus enable single-mode lasing behavior from nanowires that otherwise exhibit multimode behavior, with an concomitant increase in lasing threshold of only ~13%. These results also offer guidance for the design of metal-contacted nanoscale devices and suggest that the impact of metal contacts on the optoelectronic properties may not be as detrimental as suspected. This method should provide more flexibility in realizing practical single-mode nanowire lasers compared to alternative methods requiring nanomanipulation of

nanowires into coupled cavities or tight restrictions on the maximum nanowire diameter. It also offers insight into the design of metal-contacted nanoscale optoelectronics.

Chapter 6

Polarization Study of GaN Nanowire Lasers

Semiconductor nanowires are quasi-one-dimensional structures with unique optical properties such as wave-guiding, photon confinement, and being entirely composed of gain media.[16,18,67,84] Nanowire-based monochromic-coherent light sources may enable a number of groundbreaking applications, such as compact high resolution biochemical imaging and spectroscopy. For III-nitride (GaN-based) nanowires, advances in synthesis techniques[32,36-38] have given rise to high material quality and controlled nanowire geometries needed for the lasing. Moreover, increasing efforts have been dedicated recently on manipulating the fundamental lasing properties of these nanowire lasers to make them more suitable for practical applications.[52-54,57-59] However, the polarization, another key feature defining a laser emission, has rarely been studied in nanowire lasers. Polarization is essential for many practical applications. For instance, linear polarized light sources are of great importance of on-chip communication, and circularly polarized ones are crucial in chemistry and biology for detecting molecules exhibiting circular dichroism.

In this chapter, we experimentally study the polarization properties of the light emitted by a GaN nanowire laser. An experimental technique is developed to collect the light emission directly from nanowire end-facets. This technique bypasses the effect of

substrate scattering and allows for precise analysis of the light polarization from a nanowire. Laser emission with distinct light polarizations, linear and elliptical-like, is observed from an individual nanowire at different pump levels. Furthermore, a switching between these polarization states is obtained. These results offer promise for the design of novel polarized nano-scale lasers for use in polarization-sensitive applications, such as signal processing and atom-trapping.

6.1 Experimental results

The GaN nanowires are fabricated by the top-down etch approach, detailed in chapter 3. To characterize their optical properties, the nanowires are dry transferred to a secondary sapphire substrate by means of a cotton swab. To analyze the light emitted directly from the nanowire end-facets, we purposefully placed the nanowires on the edge of the substrate. The result of this transferring process can be seen in the Scanning Electron Microscope (SEM) image of Fig. 6.1(a), showing several GaN nanowires hanging (in groups and individually) at the edge of the substrate. The central nanowire is used in this work for the emission analysis. The nanowire is measured to be ~5 μm in length and ~350 nm in diameter.

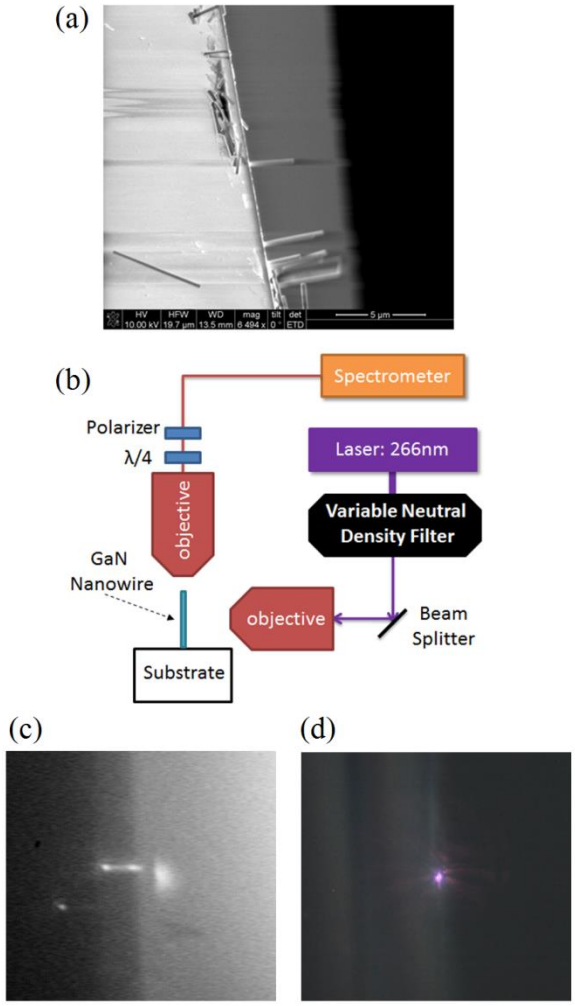

Figure 6.1(a) SEM image showing GaN nanowires placed on the edge of a cleaved substrate; (b) schematic of the experimental setup used in this work with separate excitation and analysis arms; (c and d) CCD images of individual nanowires in operation and captured from the excitation (c) and analysis (d) arms of the setup. (λ/4 ≡ Quarter-Wave Plate).

The two-arm μ-photoluminescence (μ-PL) setup, as described in chapter 3, is used to characterize the nanowire emission directly from its end-facets. Fig. 6.1(b) also shows the separated excitation and analysis arms. The two arms are orientated perpendicularly to each other so that an individual GaN nanowire can be simultaneously

optically pumped from the side and its emission collected from its end-facet. Fig. 6.1(c) and (d) respectively show CCD images of an optically-pumped GaN nanowire hanging at the substrate edge and captured respectively from the excitation (Fig. 6.1(c)) and analysis (Fig. 6.1(d)) arms of the setup. In fact, Fig. 6.1(d) shows directly the end-facet emitted light of an individual GaN nanowire (see the small purple spot at the center of the image in Fig. 1(d)). The excitation arm of the μ-PL system is composed first by a pump laser, specifically a frequency-quadrupled Nd:YAG laser operating at 266 nm (400 ps pulse duration and 10 kHz repetition rate). A variable neutral density filter wheel is also included to control the excitation strength and a 50X UltraViolet (UV) objective focuses the pumping light into a single nanowire with a pumping spot size of approximately ~5 μm in diameter. The nanowires emitted light is collected through the analysis arm of the setup. There, a 20X UV objective collects the nanowires emission which is subsequently analyzed with a 2400 groove/mm holographic grating spectrometer.

Additionally, for the analysis of the polarization properties of these nanolasers we built a rotating Quarter Wave Plate (QWP) Stokes polarimeter between the 20X UV Objective and the Spectrometer. This consist of a fixed polarizer and a rotating QWP, where varying the QWP angle from 0 to 2π radians (rads) modulates the emitted light intensity. Important polarization information, such as the Stokes parameters (S1, S2 and S3) can be extracted from this recorded intensity modulation.[85] Notice that the direct end-facet collection technique alleviates the substrate scattering effect on depolarizing the nanowire's emitted light and guarantees the accuracy of the polarization measurements.

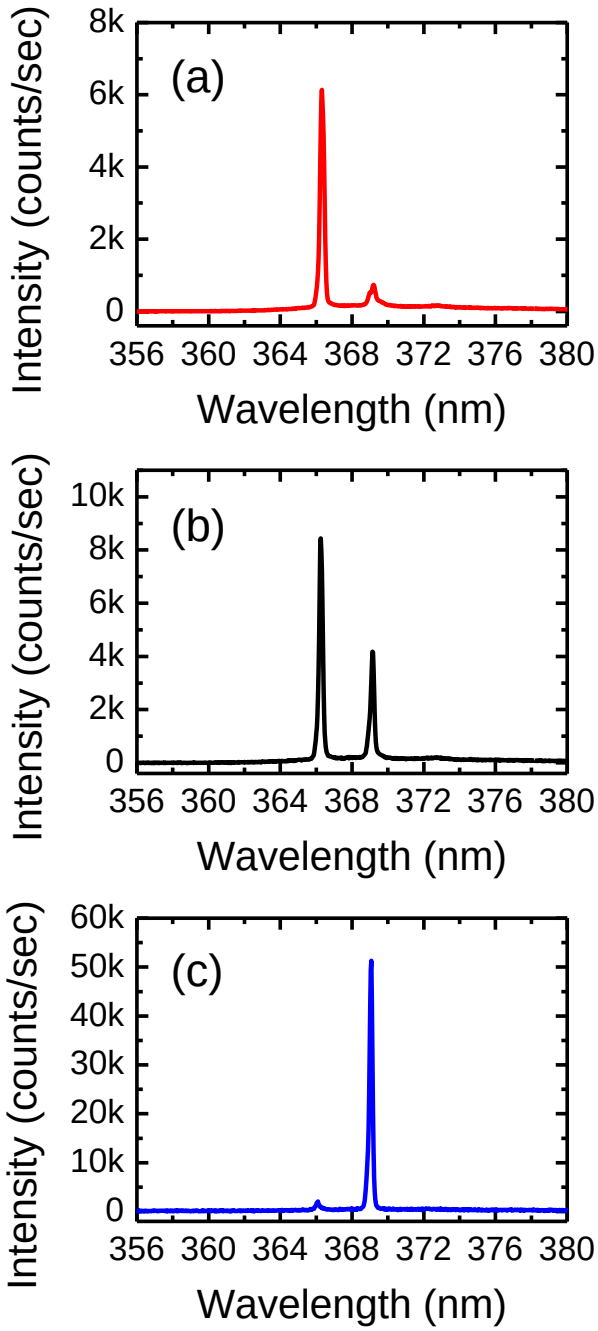

Figure 6.2 Lasing spectra collected from an end-facet of the nanowire with different excitation levels (a) 478.5 (b) 580 and (c) 1242 kW/cm^2.

When optically exited above threshold, the nanowire laser demonstrates dual-wavelength operation at 366 and 369 nm, and a switch of the lasing wavelength from 366

to 369 nm is observed with the increase of the pump power. Fig. 6.2 shows optical spectra measured from the nanowire end-facet emission at excitation levels at 478.5 kW/cm^2 [Fig. 6.2(a)], 580 kW/cm^2 [Fig. 6.2(b)] and 1242 kW/cm^2 [Fig. 6.2(c)] (all exceeding the threshold for lasing). At a low pump power, the nanowire lasing at 366 nm dominates as shown in Fig. 6.2(a). Interestingly, when the pump power is increased, the lasing peak at 369 nm increases more rapidly than that at 366 nm, indicated in Fig. 6.2(b). From this point, keep increasing the pump power leads to the shift of the dominating lasing wavelength to 366 nm.

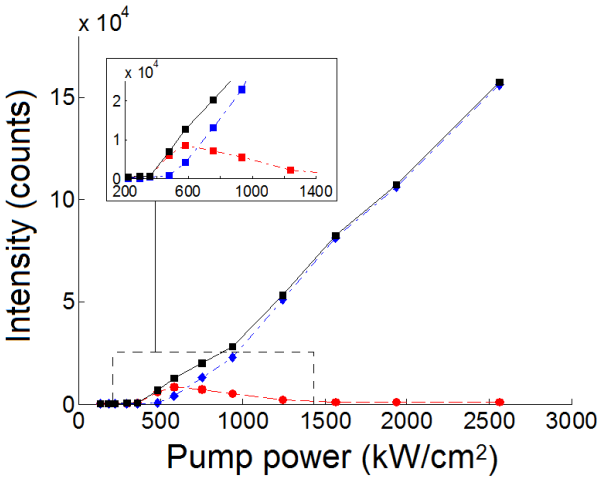

Figure 6.3 Total (black curve) and mode-resolved (red and blue curves) Light-Power (L-P) characteristics of the analyzed GaN nanowire laser; Red/Blue curves show results for the SW/LW lasing component. The inset shows in detail the lasing threshold region.

The switching of the lasing wavelength was further studied by measuring the Light-Power (L-P) characteristic of the GaN nanowire laser. Fig. 6.3 shows the obtained results from the nanowire end-facet emission with both the polarizer and QWP set at their respective fast-axes so that the intensity of the two spectral peaks is not changed related

to each other. Red and blue curves depict respectively the resolved L-P characteristics for the short-wavelength (SW) and long-wavelength (LW) lasing lines. The black curve plots the total intensity, defined as the sum of the intensities of both lasing components. The inset in Fig. 6.3 shows more details in the lasing threshold region. Fig. 6.3 shows that after a first threshold in excitation level of approximate 350 kW/cm^2, the nanowire starts lasing in the SW component (in red). Then, exceeding a second threshold (around 500 kW/cm^2) the LW line also starts to lase. For a small range of excitation both lasing lines co-exist simultaneously. However, the LW line results quickly favored and its emission increases gradually with increased excitation. Meanwhile, the intensity of the SW lasing line saturates and decays gradually until levels much smaller than those measured for the LW component.

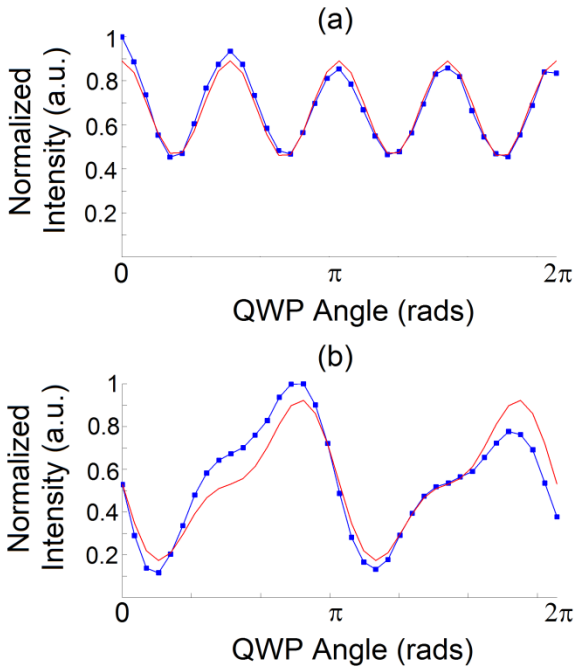

Figure 6.4 Measured (blue) and calculated (red) normalized optical intensity vs. QWP angle relationships for the SW (a) and LW (b) lasing lines emitted by the GaN nanowire laser.

Two conclusions can be therefore extracted from the L-P characteristics in Fig. 6.3: first, different lasing components with different thresholds occur in the analyzed GaN nanowire laser; second, switching between these two lasing components with an associated emission wavelength switching is produced for increasing excitation levels.

To further clarify the lasing characteristics, the polarization properties of the two lasing components of the GaN nanowire laser are also analyzed by means of the QWP Stokes polarimeter. Complete details on the working mechanism of the polarimeter as well as on the equations to extract the Stokes polarization parameter values can be found in Ref. 85. In this work, the polarization of each spectral lasing peaks can be analyzed separately by simply taking the spectral intensity of each individually peak for the polarization analysis. Fig. 6.4(a) and (b) plot the measured optical intensity versus QWP angle relationship for the SW and LW lasing lines respectively (blue curves). In these plots, the optical intensity is normalized with the maximum peak power during the rotation of the QWP. It is seen the blue curve in Fig. 6.4(a) fit well with a sinusoidal intensity modulation (red curve) with a $\pi/2$ radians period for the SW lasing line of the nanowire, which is indicative of a linear polarization for the SW lasing component [15]. The blue curve in Fig. 6.4(b) fits with intensity curve (red) showing a distinctly different behavior with intensity minima separated by π radians and two sinusoidal components which are shifted by $\pi/2$ radians, which is characteristic of elliptically polarized emission for the LW lasing components.[85]

Furthermore, we calculate the Stokes parameter values and used them to generate Poincare spheres plotting the polarization states of the SW [Fig. 6.5(a)] and LW [Fig. 6.5(b)] lasing lines. As predicted, the red dot appearing in the equator of the sphere in Fig.

5(a) indicates linearly polarized emission. On the other hand, the LW lasing component is elliptically polarized as indicated by the blue dot which is located now at the rear side and in the southern hemisphere of the Poincare sphere of Fig. 6.5(b). Fig. 6.3-6.5 therefore reveal not only a switching of lasing wavelength, but also a switching of lasing polarization with increasing excitation.

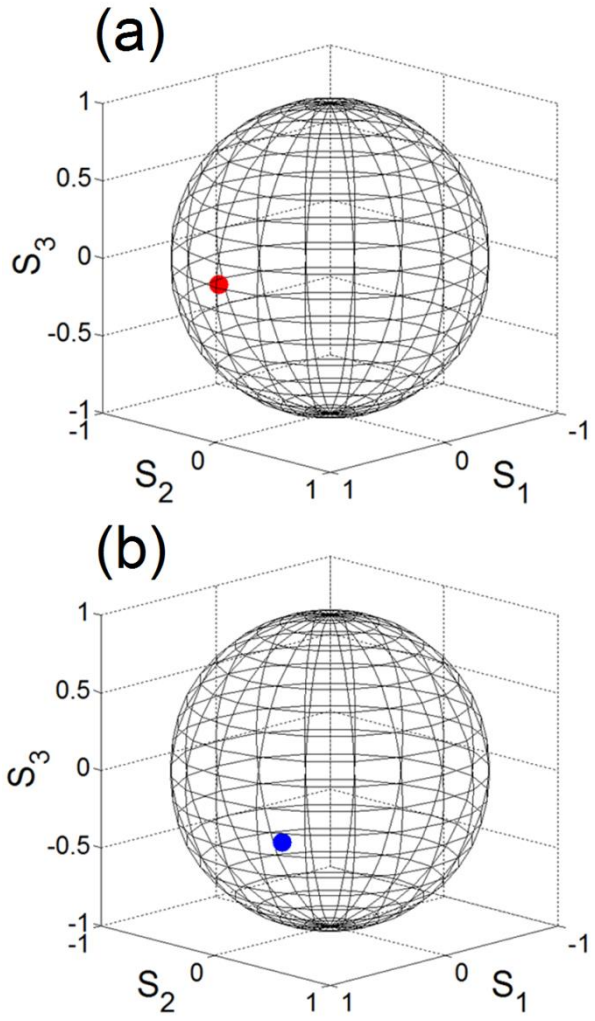

Figure 6.5 Poincare spheres depicting the polarization state for the two lasing lines emitted by the GaN nanowire. (a) SW and (b) LW lines.

6.2 Discussions

The switching of the lasing wavelength and polarization can be ascribed to the change of lasing transverse modes in the nanowire. Since the operation wavelength is comparable to the nanowire diameter it functions as a multimode waveguide.[33,34] In a nanowire with a circularly cross-sectional geometry, the first three lowest transverse modes (HE_{11}, TE_{01}, and TM_{01}) are considered as the candidates to lase due to their greater mode confinement compared with the higher order modes.[49,50] Oppositely to the HE_{11} mode which is linearly polarized, the TE_{01} and TM_{01} modes have vector polarization states, azimuthally and radially polarized respectively.[86] Due to the symmetrical distribution of the modes with vector polarization, they should exhibit a circular polarization when measured with the polarimeter of this work. However, imperfections in the NW's geometry can distort the mode distribution, resulting in a change of the measured polarization from circular to elliptical. From the discussion above, we believe that the SW lasing peak corresponds to the EH_{11} mode whereas the LW lasing line corresponds to the TE_{01} mode or TM_{01} mode.

The switching between the two lasing modes arises from the different cavity losses of each transverse mode. The threshold equation for a free-standing NW laser can be expressed as $\Gamma g_{th} = \alpha_R + \alpha_W$, where Γ is the photonic confinement factor, g_{th} is the threshold material gain, and α_R and α_W stand respectively for the reflection and waveguide losses. Theoretical analyses have revealed that α_R varies for different transverse modes with TE_{01} mode possessing the lowest value of α_R due to its highest end-facet reflectivity.[49] This mode has thereby been predicted to lase first in a nanowire laser. However, our experimental results differ from this theoretical prediction, where the HE_{11} mode exhibits a lowest lasing threshold. It is believed that this difference can be

attributed to sidewall and end-facet defects in the NW which cause the TE_{01} mode to experience a larger α_W than that of the HE_{11} mode. These are likely to happen during fabrication and also during the transferring process to the secondary substrate for analysis (either while chopping their down with the razor blade or when affixing them to the substrate's edge with the cotton swab). It is finally believed that the observed transverse-mode switching with the associated emitted light polarization switching is due to the mode competition.

6.3 Summary

In this chapter, The polarization properties of a GaN nanowire laser are studied experimentally by direct analysis of light emission from the nanowire end-facets. This technique alleviates the effect of substrate scattering on depolarizing the light emission from the nanowire, which ensures the precise polarization measurements in the experiment. Linearly and elliptically polarized emissions are both obtained in a single nanowire, and a clear switching of the polarization states is observed with the change of optical excitation. The polarization switching of the nanowire is accompanied with a corresponding lasing wavelength change from 366 to 369 nm. This polarization and wavelength switching is attributed to a transferring of transverse modes from a linear polarized fundamental HE mode to a TE or TM mode, which originates from their difference in cavity loss. This work deepens in the analysis of the emission properties of GaN nanowire lasers and offers promise for the design of polarization controlled nanolasers for polarization-sensitive applications as well as nonlinear elements for all-optical signal processing at the nanoscale.

Chapter 7

Polarization Control of GaN Nanowire Lasers

The polarization properties of a typical GaN nanowire laser is introduced in Chapter 6. It is found that a free-standing GaN nanowire can emit with different polarization states, and the polarization of the nanowire can be switched from one state to another with the variation of pump strength. Apparently, this randomly polarized lasing is not suitable for many practical applications that need stable and specifically polarized light emission. For this reason, it is required to develop polarization control techniques for realizing stable and specific polarization states.

In this chapter we present a polarization control approach in optically-pumped individual GaN nanowire lasers. By simply placing the GaN nanowires onto gold substrates, the naturally occurring randomly orientated elliptical polarization of the nanowire lasers can be converted to a linear polarization that is strictly oriented parallel to the substrate surface. Confirmed by the simulation results, this polarization control is attributed to a polarization-dependent loss induced by the gold substrate, which breaks the mode degeneracy of the nanowire and forms two orthogonally polarized modes with largely different cavity losses.

7.1 Experimental results

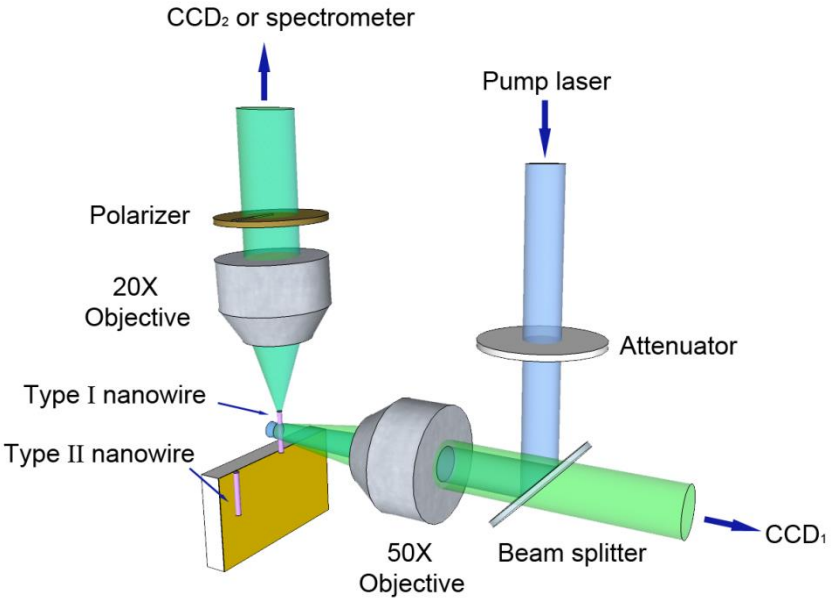

Figure 7.1 Schematic of the two-arm micro-PL setup. In the pump arm (right), an incident laser beam pumps the GaN nanowires from the side. In the collection arm (left), the objective is aligned along the nanowire axis so that its polarization can be measured accurately.

The GaN nanowires investigated in this work are fabricated using a top-down dry plus wet-etch technique, detailed in Chapter 3. The GaN nanowires are dry-transferred onto target substrates for optical characterization. Firstly, a cotton swab is used to rub the surface of the fabricated nanowire samples. As a result, GaN nanowires cleave at the sapphire/GaN interface and affix to the swab. The swab is then gently dabbed at the edge of the target substrates to transfer the nanowires onto them. In this work, a Si(100) wafer covered by a 200 nm thick gold film is used as the target substrate. After the dry transfer is performed, two types of nanowires are selected for analysis. As illustrated in Fig. 7.1, Type I nanowires hang over the edge of the substrate with minimal contact area to the

substrate; Type II nanowires contact the substrate along their entire length. Type I and II nanowires are subsequently characterized by means of a two-arm micro photoluminescence (PL) system. As seen in Fig. 7.1, the pump arm of the PL system consists of a pump laser, an attenuator, and a 50X objective. The pump laser is a frequency-quadrupled Nd:YAG laser operating at 266 nm with a 400 ps pulse duration and a 10 kHz repetition rate. The pump spot size is approximately ~5 μm in diameter. A nanowire is optically excited from this pump arm and its light emission is collected by the other arm (collection arm), which includes a 20X objective, a polarizer, and a 300 mm spectrometer with a 2400 groove/mm holographic grating. The collection arm is orientated perpendicular to the pump arm so that the nanowires can be pumped from the side and at the same time their emission can be collected directly from the end facets. Note that the direct collection technique alleviates the substrate scattering effect on depolarizing the nanowire emission, ensuring the accuracy of the polarization measurements. The polarization of the nanowire laser is studied by adjusting the angle of the polarizer and analyzing the light power that propagates through it.

Fig. 7.2(a) shows a scanning electron microscopic (SEM) image of a type I nanowire. As is seen in this figure that the nanowire barely contacts the substrate surface, resulting in a negligible substrate effect. The nanowire is 5 μm in length and 225 nm in diameter. By uniformly illuminating the nanowire and gradually increasing the pumping power, lasing behavior of the nanowire is observed with a threshold of 246 kW/cm^2. This achievement of lasing threshold is experimentally evidenced by a sudden spectral narrowing, a transition from uniform body emission to a high contrast end-facet emission, and an interference pattern generation.[32] Fig 7.2(b) shows a lasing spectrum from this

nanowire obtained at 359 kW/cm^2, exhibiting single-mode lasing with a bandwidth of ~0.15 nm (limited by the resolution of the spectrometer). Our previous work has revealed that this single-wavelength lasing originates from the narrow material gain spectrum and the short nanowire cavity length, which lead to a strong mode competition.[32] Fig. 7.2(c) shows a SEM image of a type II GaN nanowire with similar dimensions to those of the previously discussed type I nanowire. Fig. 7.2(d) shows a lasing spectrum of the nanowire obtained at 389 kW/cm^2, which shows a similar single-wavelength lasing behavior. From the comparison of the spectra and threshold values, it can be concluded that the two types of nanowires presents similar lasing behaviors.

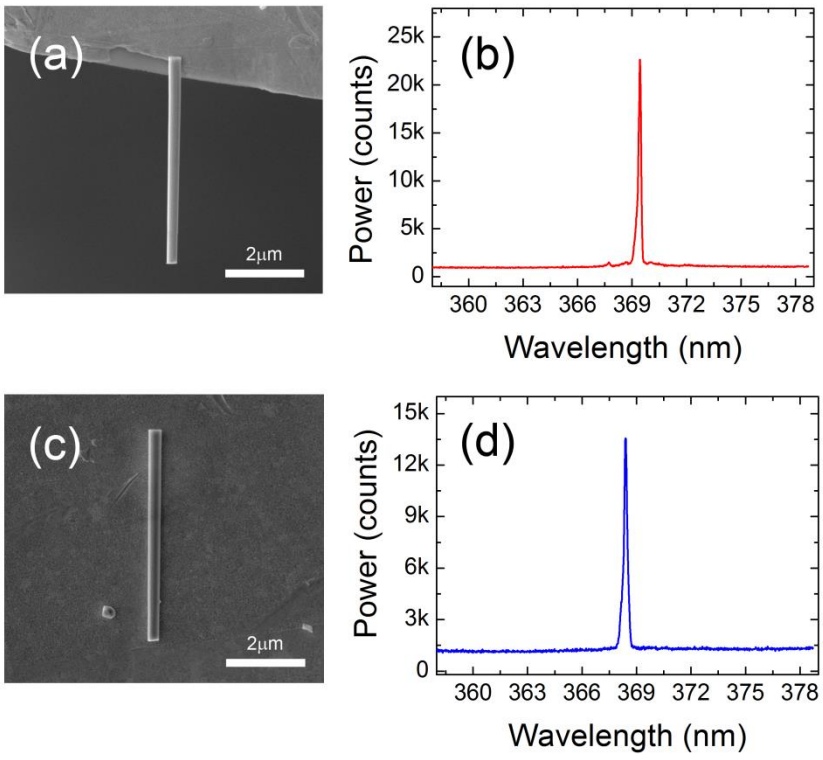

Figure 7.2 (a) SEM image and (b) lasing spectrum of a nanowire hanging over the substrate edge; (c) SEM image and (d) lasing spectrum of a nanowire lying on the substrate surface.

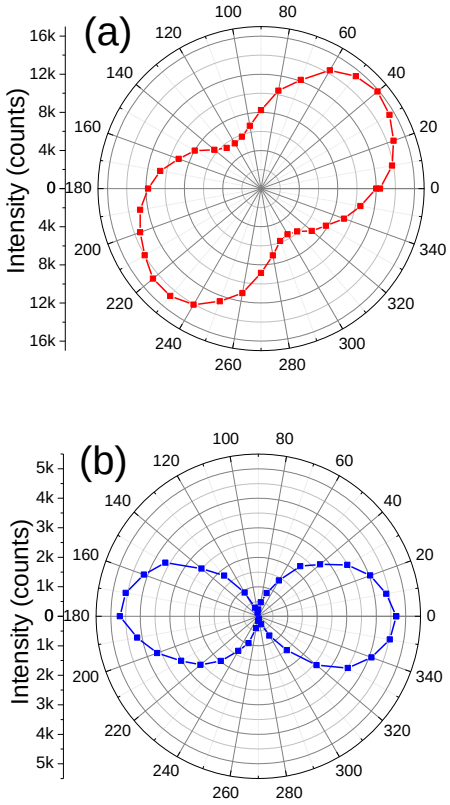

Figure 7.3 Optical power versus polarizer rotation angle measured for (a) the hanging nanowire (type I) and (b) the nanowire placed onto the gold substrate (type II). The $0^o/90^o$ indicates the orientation parallel/perpendicular to the substrate surface.

However, the analysis of the polarization properties of these two types of nanowire lasers reveal distinct differences. Fig. 7.3(a) shows the measured lasing emission power of the type I nanowire as a function of the polarizer rotation angle. A "peanut shaped" plot is obtained with clear maximum and minimum axes at ~36^o and ~126^o respectively. Additionally, the cross-polarization suppression ratio (CPSR) is measured to be 2.7:1. These features reveal that this nanowire (Type I) emission is elliptically-like polarized. In contrast, Fig. 7.3(b) shows that a highly linear polarized emission is observed for the type II nanowire laser. The CPSR of this nanowire laser reaches a value as high as ~23:1.

Moreover, its major polarization axis is measured to be -2°, evidencing that the type II laser polarization is parallel to the substrate surface.

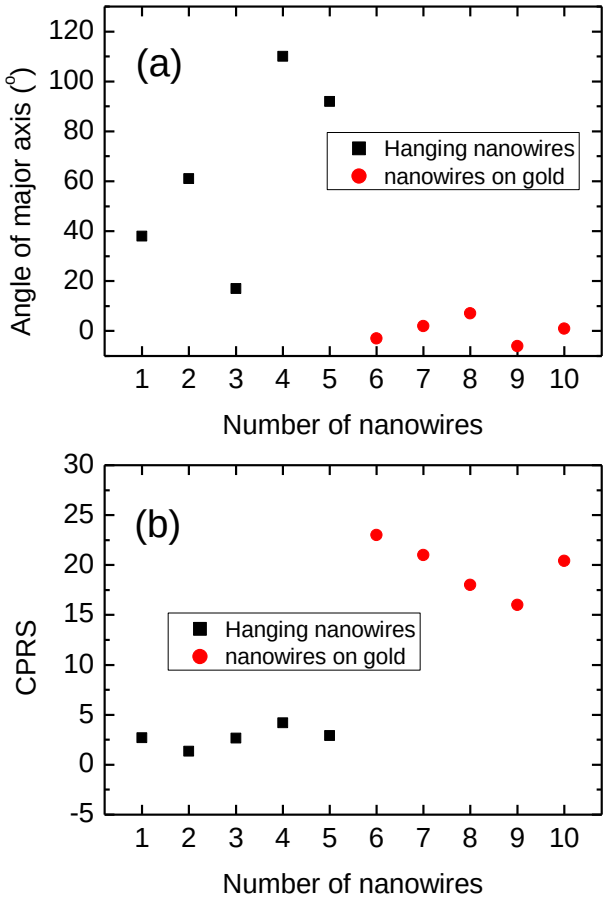

Figure 7.4 Statistics of (a) polarization major axes and (b) CPSRs from 10 nanowires with similar geometry.

This experiment is further repeated on 10 more GaN nanowire lasers (5 type I and 5 type II). The statistical analysis of the major polarization axes and the CPSRs of these nanowire lasers are summarized in Fig. 7.4. From Fig. 7.4(a), a mean axis of 63.6° is calculated with a standard deviation of 38.06° for the type I nanowire. This result confirms a random polarization angle from type I nanowires. In contrast, type II nanowires have a mean axis of 0.2° with a standard deviation of 4.96°, suggesting a fixed

polarization parallel to the substrate surface. Note that the uniformity of the nanowires, the substrate surface roughness, and the alignment of the nanowires with the collection arm all contribute to the deviation of polarization orientation. Moreover, from Fig. 7.4(b), type II nanowires show an average CPSR of 20, much larger than those of the type I nanowires. These statistical results reveal that the gold substrate leads to linear and substrate-parallel polarization in GaN nanowire lasers.

7.2 Simulation results and discussions

The difference in polarization properties of the nanowire-substrate configurations can be attributed to a polarization-dependent loss generated by the gold substrate. Due to the negligible substrate effect, type I nanowires are axially symmetric. Therefore, they may support degenerate modes with different polarization simultaneously, forming the elliptically polarized laser emission. Another possible reason for the obtained elliptical-like polarization state is the TE_{01} or TM_{01} mode operation of such nanowire lasers, as described in Chapter 6. In contrast, when the lossy gold substrate is present, the fundamental HE_{11} mode will be favored to lase due to its lower cavity loss (this result is obtained in Chapter 5). Moreover, with the presence of the gold substrate, the mode degeneracy is broken, and difference cavity losses can be expected for differently polarized modes. To clarify the gold substrate effect on the polarization of the nanowire lasers, we conduct simulations to illustrate the modal properties of GaN nanowires placed on a gold substrate. The nanowire passive eigenmodes are determined using a fully vectorial commercial Eigenmode Solver from Lumerical Inc In the simulation, the operation wavelength is set to 367 nm, the real part and imaginary part of gold respectively are set to 1.70 and 1.88[83], and the refractive index of GaN is set to 2.67[71].

Fig. 7.5 shows two orthogonally polarized HE_{11} modes supported by this nanowire/gold-substrate geometry. These two modes are polarized parallel and perpendicular to the substrate, respectively. In spite of the similar mode distributions, these two modes show large difference in propagation loss, i.e., the propagation loss for the parallel polarized mode (Fig. 7.5(a)) is 0.36 dB/μm, which is significantly lower than 2.11 dB/μm for the perpendicularly polarized mode (Fig. 7.5(b)). The large cavity loss difference suppresses the perpendicular cavity mode and clamps the polarization parallel to the substrate.

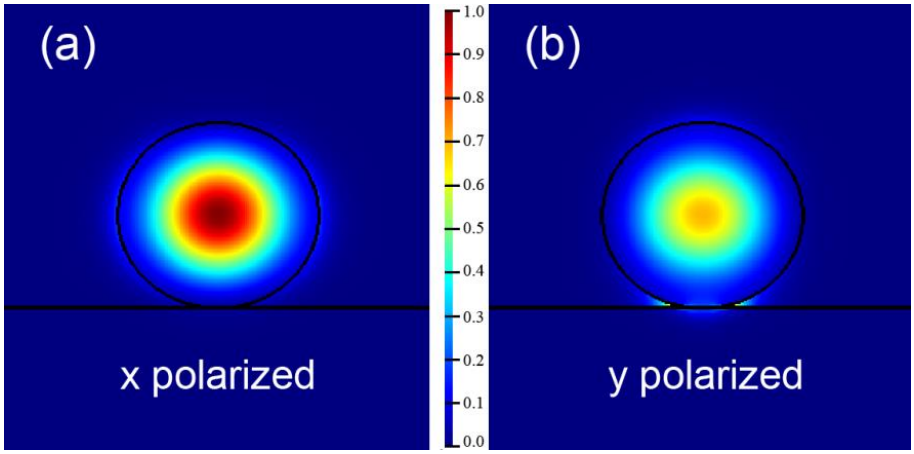

Figure 7.5 Mode intensity distributions calculated for a 230 nm diameter GaN nanowire placed on a gold substrate, i.e. distribution of the mode with polarization parallel (a) and perpendicular (b) to the substrate.

7.3 Summary

In this chapter, we demonstrate polarization control of optically pumped individual GaN nanowires with the utilization of a gold substrate. The gold substrate breaks the mode degeneracy of a nanowire and form two orthogonally polarized modes with a large difference in cavity loss. This polarization-dependent cavity loss suppresses the perpendicular polarized mode, leading to a linearly polarized lasing with polarization

orientation parallel to the substrate surface. These results represent a drastic contrast with the randomly oriented elliptical polarization laser emission observed from GaN nanowires without the loss mechanism. Our technique offers a simple methodology for controlling the polarization of individual nanowire lasers without drastically altering the performance of individual devices.

Chapter 8 Conclusion and Future Work

While GaN nanowire lasers naturally operate in a combined multi-mode and randomly polarized state, controlled lasing is desired for many practical applications. This dissertation exerts efforts on the study of fundamental lasing characteristics and their control in these nanowires, and demonstrates the following results.

Stable single-mode lasing operation is realized from a pair of coupled GaN nanowires through optical pumping. By placing two nanowires side-by-side in contact, the resulting coupled cavity generates a Vernier effect, which dramatically increases the spectral spacing between adjacent resonant modes, giving rise to the simultaneous suppression of multi-transverse and multi-longitudinal mode operation. By this approach, single-mode lasing is obtained from coupled nanowires with large diameters.

A flexible approach for achieving single-mode lasing in the GaN nanowires is also demonstrated by coupling an individual nanowire, which otherwise exhibits multimode lasing properties, to a underlying gold substrate. As illustrated by the simulation results, the difference in the spatial distribution of different transverse modes causes them to be attenuated differently by the presence of the metal (high-order transverse modes have much larger attenuation compared with the fundamental mode). Therefore, the nanowire-gold contact generates a mode-dependent loss, which can strongly attenuate higher modes and ensure the single-mode operation.

Polarization properties of a GaN nanowire laser are also experimentally studied by direct analysis of its end-facet emission. Linear and elliptical light polarization states are both obtained from a single nanowire at different pump strength. A switching between these two polarization states is also observed with the adjustment of the optical excitation. This polarization switching is attributed to a variation of lasing transverse modes, which originates from the difference of cavity losses for these transverse modes.

Furthermore, lasing polarization control is achieved by the coupling of the GaN nanowire lasers to an underlying gold substrate. The gold substrate breaks the degeneracy symmetry of the nanowire geometry and generates an inherent polarization-sensitive loss. By simply placing the GaN nanowires onto gold substrates, the naturally occurring randomly orientated elliptical polarization of the nanowire lasers can be converted to a linear polarization that is strictly oriented parallel to the substrate surface.

What of special interest for the future work is the demonstration of mode-locked nanowire lasers. Integration of a semiconductor nanowire with a certain saturable absorber, such as graphene, may lead to demonstration of smallest mode-locked lasers. Such lasers is promising in terms of their ultra-small dimensions and much higher repetition rate pulse generation compared with all the existing mode-locked lasers.

Also of interest is the metal-nanowire contacted nanodevices. As demonstrated in the dissertation, a metal substrate has effects on both mode selection and polarization control for the nanowire lasers. Enlightened from this, single nanodevices might be obtainable by the integration of single nanowires with specifically patterned metal coating on the nanowire surfaces. For instance, from the simulation results, we find that

single EH_{11} mode lasing with controlled polarization can be generated from a GaN nanowire with a line (~50 nm width) of gold deposited on the nanowire along its axis. These metal-nanowire contact designs may open promising to demonstrate novel-featured devices.

In addition, the future work also involves the demonstration of electrical injected nanowire lasers, GaN nanodisk lasers, and various nanodevices with III-nitride heterostructures, such as the core-shell nanowire lasers.

List of Publications

1. **H. Xu**, A. Hurtado, J. B. Wright, C. Li, S. Liu, J. J. Figiel, K. Cross, G. T. Wang, T. S. Luk, S. R. J. Brueck, I. Brener, L. F. Lester, G. Balakrishnan, and Q. Li, Manipulating the polarization of GaN nanowire lasers, submitted to Applied Physics Letters.

2. A. Hurtado, **H. Xu**, J. B. Wright, S. Liu, Q. Li, G. T. Wang, T. S. Luk, J. J. Figiel, K. Cross, G. Balakrishnan, L. F. Lester, and I. Brener, Polarization switching in GaN nanowire lasers, in prepare.

3. J. B. Wright, S. Liu, G. T. Wang, Q. Li, A. Benz, D. D. Koleske, P. Lu, **H. Xu**, L. L, T. S. Luk, I. Brener, and G. S. Subramania, Multi-color III-nitride photonic crystal nanowire laser array on a single chip, submitted to Nature Scientific Reports.

4. J. B. Wright, S. Liu, J. Martinez, **H. Xu**, T. S. Luk, Q. Li, G. T. Wang, I. Brener, and L. F. Lester, Gallium nitride distributed feedback nanowire lasers, in prepare.

5. E. B. Malm, N. C. Monserud, C. G. Brown, P. W. Wachulak, **H. Xu**, G. Balakrishnan, W. chao, E. Anderson, and M. C. Marconi, Tabletop single-shot extreme ultraviolet Fourier transform holography of an extended object, Optics Express, **21**(8), 9959 (2013)

6. **H. Xu**, J. B. Wright, T. S. Luk, J. J. Figiel, K. Cross, L. F. Lester, G. Balakrishnan, G. T. Wang, I. Brener, and Q. Li, Single-mode lasing of GaN nanowire-pairs, Applied Physics Letters **101** (11), 113106 (2012).

7. **H. Xu**, J. B. Wright, A. Hurtado, Q. Li, T.-S. Luk, J. J. Figiel, K. Cross, G. Balakrishnan, L. F. Lester, and I. Brener, Gold substrate-induced single-mode lasing of GaN nanowires, Applied Physics Letters **101** (22), 221114 (2012).

8. Q. Li, J. J. Figiel, G. T. Wang, **H. Xu**, and G. Balakrishnan, GaN epitaxy on Cu(110) by metal organic chemical vapor deposition, Appl. Phys. Lett. **100**, 192110 (2012)

9. D. Brake, **H. Xu**, A. Hollowell, G. Balakrishnan, C. Hains, M. Marconi, and V. Putkaradze, Intrinsic localized modes in two-dimensional vibrations or crystalline pillars and their applications for sensing, J. Appl. Phys. **112**, 104326 (2012)

List of Presentations

1. **H. Xu**, J. B. Wright, A. Hurtado, T. S. Luk, J. J. Figiel, L. F. Lester, I. Brener, Q. Li, and G. T. Wang, Mode and polarization control in gallium nitride nanowire lasers, 10th International Conference on Nitride Semiconductors, Aug. 25-30, (2013).
2. **H. Xu**, J. B. Wright, T. S. Luk, J. J. Figiel, K. Cross, L. F. Lester, G. Balakrishnan, G. T. Wang, I. Brener, and Q. Li, Single-mode lasing in gallium nitride nanowires, SPIE Photonics West 2013, San Francisco, Feb. 3-6 (2013).
3. **H. Xu**, J. B. Wright, T. S. Luk, J. J. Figiel, K. Cross, L. F. Lester, G. Balakrishnan, G. T. Wang, I. Brener, and Q. Li, Mode control in gallium nitride nanowire lasers, 55th Electronic Materials Conference, South Bend, Jun. 26-28 (2013)
4. **H. Xu**, A. Hurtado, J. B. Wright, C. Li, S. Liu, J. J. Figiel, K. Cross, G. T. Wang, T. S. Luk, S. R. J. Brueck, I. Brener, L. F. Lester, G. Balakrishnan, and Q. Li, Manipulation of lasing polarization in GaN nanowire lasers, 55th Electronic Materials Conference, South Bend, Jun. 26-28 (2013).
5. J. B. Wright, S. Liu, G. T. Wang, Q. Li, A. Benz, D. D. Koleske, P. Lu, **H. Xu**, L. L, T. S. Luk, I. Brener, and G. S. Subramania, Multi-color III-nitride photonic crystal nanowire laser array on a single chip, 55th Electronic Materials Conference, South Bend, Jun. 26-28 (2013).
6. A. Hurtado, **H. Xu**, J. B. Wright, S. Liu, Q. Li, G. T. Wang, T. S. Luk, J. J. Figiel, K. Cross, G. Balakrishnan, L. F. Lester, and I. Brener, Polarization properties of GaN nanowire lasers, CLEO 2013, San Jose, Jun. 9-14, (2013).
7. J. B. Wright, S. Liu, G. T. Wang, Q. Li, A. Benz, D. D. Koleske, P. Lu, **H. Xu**, L. L, T. S. Luk, I. Brener, and G. S. Subramania, Multi-color III-nitride photonic crystal nanowire laser array on a single chip, CLEO 2013, San Jose, Jun. 9-14, (2013).

8. J. B. Wright, S. Liu, J. Martinez, **H. Xu**, T. S. Luk, Q. Li, G. T. Wang, I. Brener, and L. F. Lester, Gallium nitride distributed feedback nanowire lasers, CLEO 2013, San Jose, Jun. 9-14, (2013).

9. Q. Li, **H. Xu**, J. J. Figiel, G. T. Wang, G. Balakrishnan, GaN epitaxy on Cu(110) by MOCVD, 54th Electronic Materials Conference, Pennsylvania, Jun. 20-22 (2012).

10. Q. Li, J. B. Wright, **H. Xu**, J. J. Figiel, K. Cross, D. Koleske, G. T. Wang, I. Brener, T. S. Luk, W. Chow, Single mode GaN nanowire lasers, 2012 MRS Spring Meeting & Exhibit, San Francisco, April 9-13 (2012)

References

[1] Y. Gu, E.-S. Kwak, J. Lensch, J. Allen, T. W. Odom, and L. J. Lauhon, Near-field scanning photocurrent microscopy of a nanowire photodetector, Applied Physics Letters **87** (4), 043111 (2005).

[2] J. Law and J. Thong, Simple fabrication of a ZnO nanowire photodetector with a fast photoresponse time, Applied Physics Letters **88** (13), 133114 (2006).

[3] C. Soci, A. Zhang, B. Xiang, S. A. Dayeh, D. Aplin, J. Park, X. Bao, Y.-H. Lo, and D. Wang, ZnO nanowire UV photodetectors with high internal gain, Nano Letters **7** (4), 1003 (2007).

[4] J. Wang, M. S. Gudiksen, X. Duan, Y. Cui, and C. M. Lieber, Highly polarized photoluminescence and photodetection from single indium phosphide nanowires, Science **293** (5534), 1455 (2001).

[5] G. Zheng, F. Patolsky, Y. Cui, W. U. Wang, and C. M. Lieber, Multiplexed electrical detection of cancer markers with nanowire sensor arrays, Nature biotechnology **23** (10), 1294 (2005).

[6] Q. Wan, Q. Li, Y. Chen, T. Wang, X. He, J. Li, and C. Lin, Fabrication and ethanol sensing characteristics of ZnO nanowire gas sensors, Applied Physics Letters **84** (18), 3654 (2004).

[7] B. Wang, L. Zhu, Y. Yang, N. Xu, and G. Yang, Fabrication of a SnO2 nanowire gas sensor and sensor performance for hydrogen, The Journal of Physical Chemistry C **112** (17), 6643 (2008).

[8] A. B. Greytak, C. J. Barrelet, Y. Li, and C. M. Lieber, Semiconductor nanowire laser and nanowire waveguide electro-optic modulators, Applied Physics Letters **87**, 151103 (2005).

[9] J. C. Johnson, H. Yan, P. Yang, and R. J. Saykally, Optical cavity effects in ZnO nanowire lasers and waveguides, The Journal of Physical Chemistry B **107** (34), 8816 (2003).

[10] J. Bao, M. A. Zimmler, F. Capasso, X. Wang, and Z. Ren, Broadband ZnO single-nanowire light-emitting diode, Nano Letters **6** (8), 1719 (2006).

[11] R. Konenkamp, R. C. Word, and C. Schlegel, Vertical nanowire light-emitting diode, Applied Physics Letters **85** (24), 6004 (2004).

[12] S. Hersee, M. Fairchild, A. Rishinaramangalam, M. Ferdous, L. Zhang, P. Varangis, B. Swartzentruber, and A. Talin, GaN nanowire light emitting diodes based on templated and scalable nanowire growth, Electronics Letters **45** (1), 75 (2009).

[13] Q. Li, K. R. Westlake, M. H. Crawford, S. R. Lee, D. D. Koleske, J. J. Figiel, K. C. Cross, S. Fathololoumi, Z. Mi, and G. T. Wang, Optical performance of top-down fabricated InGaN/GaN nanorod light emitting diode arrays, Optics Express **19** (25), 25528 (2011).

[14] H. Jiang, S. Jin, J. Li, J. Shakya, and J. Lin, III-nitride blue microdisplays, Applied Physics Letters **78** (9), 1303 (2001).

[15] J. Day, J. Li, D. Lie, C. Bradford, J. Lin, and H. Jiang, III-Nitride full-scale high-resolution microdisplays, Applied Physics Letters **99** (3), 031116 (2011).

[16] X. Duan, Y. Huang, R. Agarwal, and C. M. Lieber, Single-nanowire electrically driven lasers, Nature **421** (6920), 241 (2003).

[17] J. C. Johnson, H.-J. Choi, K. P. Knutsen, R. D. Schaller, P. Yang, and R. J. Saykally, Single gallium nitride nanowire lasers, Nature Materials **1** (2), 106 (2002).

[18] M. H. Huang, S. Mao, H. Feick, H. Yan, Y. Wu, H. Kind, E. Weber, R. Russo, and P. Yang, Room-temperature ultraviolet nanowire nanolasers, Science **292** (5523), 1897 (2001).

[19] J. C. Johnson, H. Yan, R. D. Schaller, L. H. Haber, R. J. Saykally, and P. Yang, Single nanowire lasers, The Journal of Physical Chemistry B **105** (46), 11387 (2001).

[20] L. Tsakalakos, J. Balch, J. Fronheiser, B. Korevaar, O. Sulima, and J. Rand, Silicon nanowire solar cells, Applied Physics Letters **91**, 233117 (2007).

[21] A. L. Briseno, T. W. Holcombe, A. I. Boukai, E. C. Garnett, S. W. Shelton, J. J. Fréchet, and P. Yang, Oligo-and polythiophene/ZnO hybrid nanowire solar cells, Nano Letters **10** (1), 334 (2009).

[22] M. Law, L. E. Greene, J. C. Johnson, R. Saykally, and P. Yang, Nanowire dye-sensitized solar cells, Nature Materials **4** (6), 455 (2005).

[23] J. J. Wierer, Q. Li, D. D. Koleske, S. R. Lee, and G. T. Wang, III-nitride core–shell nanowire arrayed solar cells, Nanotechnology **23** (19), 194007 (2012).

[24] H. Rong, Y.-H. Kuo, A. Liu, M. Paniccia, and O. Cohen, High efficiency wavelength conversion of 10 Gb/s data in silicon waveguides, Optics Express **14** (3), 1182 (2006).

[25] D.-I. Yeom, E. C. Mägi, M. R. Lamont, M. A. Roelens, L. Fu, and B. J. Eggleton, Low-threshold supercontinuum generation in highly nonlinear chalcogenide nanowires, Optics letters **33** (7), 660 (2008).

[26] P. J. Pauzauskie and P. Yang, Nanowire photonics, Materials Today **9** (10), 36 (2006).

[27] P. Yang, R. Yan, and M. Fardy, Semiconductor Nanowire: What's Next?, Nano Letters **10** (5), 1529 (2010).

[28] Y. Xia, P. Yang, Y. Sun, Y. Wu, B. Mayers, B. Gates, Y. Yin, F. Kim, and H. Yan, One - dimensional nanostructures: synthesis, characterization, and applications, Advanced Materials **15** (5), 353 (2003).

[29] M. Law, J. Goldberger, and P. Yang, Semiconductor nanowires and nanotubes, Annu. Rev. Mater. Res. **34**, 83 (2004).

[30] Y. Huang and C. M. Lieber, Integrated nanoscale electronics and optoelectronics: Exploring nanoscale science and technology through semiconductor nanowires, Pure and applied chemistry **76** (12), 2051 (2004).

[31] Y. Inoue, T. Hoshino, S. Takeda, K. Ishino, A. Ishida, H. Fujiyasu, H. Kominami, H. Mimura, Y. Nakanishi, and S. Sakakibara, Strong luminescence from dislocation-free GaN nanopillars, Applied Physics Letters **85** (12), 2340 (2004);

[32] Q. Li, J. B. Wright, W. W. Chow, T. S. Luk, I. Brener, L. F. Lester, and G. T. Wang, Single-mode GaN nanowire lasers, Optics Express **20** (16), 17873 (2012).

[33] H. Xu, J. B. Wright, T. S. Luk, J. J. Figiel, K. Cross, L. F. Lester, G. Balakrishnan, G. T. Wang, I. Brener, and Q. Li, Single-mode lasing of GaN nanowire-pairs, Applied Physics Letters **101** (11), 113106 (2012).

[34] H. Xu, J. B. Wright, A. Hurtado, Q. Li, T.-S. Luk, J. J. Figiel, K. Cross, G. Balakrishnan, L. F. Lester, and I. Brener, Gold substrate-induced single-mode lasing of GaN nanowires, Applied Physics Letters **101** (22), 221114 (2012).

[35] A. Hurtado, H. Xu, J. B. Wright, S. Liu, Q. Li, G. T. Wang, T. S. Luk, J. Figiel, K. Cross, and G. Balakrishnan, presented at the CLEO: Science and Innovations, 2013 (unpublished).

[36] K. A. Bertness, N. A. Sanford, and A. V. Davydov, GaN nanowires grown by molecular beam epitaxy, Selected Topics in Quantum Electronics, IEEE Journal of **17** (4), 847 (2011).

[37] D. Wang, A. Pierre, M. G. Kibria, K. Cui, X. Han, K. H. Bevan, H. Guo, S. Paradis, A. Hakima, and Z. Mi, Wafer-level photocatalytic water splitting on GaN nanowire arrays grown by molecular beam epitaxy, Nano Letters **11** (6), 2353 (2011).

[38] S. K. Lim, S. Crawford, G. Haberfehlner, and S. Gradečak, Controlled modulation of diameter and composition along individual III–V nitride nanowires, Nano Letters (2012).

[39] Y. Wu and P. Yang, Direct observation of vapor-liquid-solid nanowire growth, JOURNAL-AMERICAN CHEMICAL SOCIETY **123** (13), 3165 (2001).

[40] J. Harmand, G. Patriarche, N. Pé-Laperne, M. Mérat-Combes, L. Travers, and F. Glas, Analysis of vapor-liquid-solid mechanism in Au-assisted GaAs nanowire growth, Applied Physics Letters **87** (20), 203101 (2005).

[41] S. Y. Li, C. Y. Lee, and T. Y. Tseng, Copper-catalyzed ZnO nanowires on silicon (100) grown by vapor–liquid–solid process, Journal of Crystal Growth **247** (3), 357 (2003).

[42] X. Duan and C. M. Lieber, Laser-assisted catalytic growth of single crystal GaN nanowires, JOURNAL-AMERICAN CHEMICAL SOCIETY **122** (1), 188 (2000);

[43] R. Wagner and W. Ellis, Vapor - liquid - solid mechanism of single crystal growth, Applied Physics Letters **4** (5), 89 (1964).

[44] S. Grade ak, F. Qian, Y. Li, H.-G. Park, and C. M. Lieber, GaN nanowire lasers with low lasing thresholds, Applied Physics Letters **87** (17), 173111 (2005).

[45] Y. Wang, G. Meng, L. Zhang, C. Liang, and J. Zhang, Catalytic growth of large-scale single-crystal CdS nanowires by physical evaporation and their photoluminescence, Chemistry of materials **14** (4), 1773 (2002).

[46] Y. Xiao, C. Meng, P. Wang, Y. Ye, H. Yu, S. Wang, F. Gu, L. Dai, and L. Tong, Single-nanowire single-mode laser, Nano Letters **11** (3), 1122 (2011).

[47] E. Stern, J. F. Klemic, D. A. Routenberg, P. N. Wyrembak, D. B. Turner-Evans, A. D. Hamilton, D. A. LaVan, T. M. Fahmy, and M. A. Reed, Label-free immunodetection with CMOS-compatible semiconducting nanowires, Nature **445** (7127), 519 (2007).

[48] C. Ning, Far-field emission of a semiconductor nanowire laser, Optics letters **29** (6), 572 (2004).

[49] A. V. Maslov and C. Z. Ning, Reflection of guided modes in a semiconductor nanowire laser, Applied Physics Letters **83** (6), 1237 (2003).

[50] M. A. Zimmler, F. Capasso, S. Müller, and C. Ronning, Optically pumped nanowire lasers: invited review, Semiconductor Science and Technology **25** (2), 024001 (2010).

[51] A. Maslov and C. Ning, Modal gain in a semiconductor nanowire laser with anisotropic bandstructure, Quantum Electronics, IEEE Journal of **40** (10), 1389 (2004).

[52] M. A. Zimmler, J. Bao, F. Capasso, S. Müller, and C. Ronning, Laser action in nanowires: Observation of the transition from amplified spontaneous emission to laser oscillation, Applied Physics Letters **93** (5), 051101 (2008).

[53] P. J. Pauzauskie, D. J. Sirbuly, and P. Yang, Semiconductor nanowire ring resonator laser, Physical review letters **96** (14), 143903 (2006).

[54] L. Chen and E. Towe, Nanowire lasers with distributed-Bragg-reflector mirrors, Applied Physics Letters **89** (5), 053125 (2006).

[55] Y. Xiao, C. Meng, X. Wu, and L. Tong, Single mode lasing in coupled nanowires, Applied Physics Letters **99** (2), 023109 (2011).

[56] H. Gao, A. Fu, S. C. Andrews, and P. Yang, Cleaved-coupled nanowire lasers, Proceedings of the National Academy of Sciences **110** (3), 865 (2013).

[57] X. Liu, Q. Zhang, Q. Xiong, and T. C. Sum, Tailoring the Lasing Modes in Semiconductor Nanowire Cavities Using Intrinsic Self-Absorption, Nano Letters **13** (3), 1080 (2013).

[58] J. Li, C. Meng, Y. Liu, X. Wu, Y. Lu, Y. Ye, L. Dai, L. Tong, X. Liu, and Q. Yang, Wavelength Tunable CdSe Nanowire Lasers Based on the Absorption-Emission-Absorption Process, Advanced Materials **25** (6), 833 (2013).

[59] L. K. Van Vugt, S. Rühle, and D. Vanmaekelbergh, Phase-correlated nondirectional laser emission from the end facets of a ZnO nanowire, Nano Letters **6** (12), 2707 (2006).

[60] S. Reculusa and S. Ravaine, Synthesis of colloidal crystals of controllable thickness through the Langmuir-Blodgett technique, Chemistry of materials **15** (2), 598 (2003).

[61] J. Zhang, Y. Li, X. Zhang, and B. Yang, Colloidal Self‐Assembly Meets Nanofabrication: From Two‐Dimensional Colloidal Crystals to Nanostructure Arrays, Advanced Materials **22** (38), 4249 (2010).

[62] M. Pisco, M. Consales, A. Cutolo, A. Cusano, M. Penza, and P. Aversa, Hollow fibers integrated with single walled carbon nanotubes: bandgap modification and chemical sensing capability, Sensors and Actuators B: Chemical **129** (1), 163 (2008).

[63] Lumerical, WWW Document(www.lumerical.com).

[64] A. M. Morales and C. M. Lieber, A laser ablation method for the synthesis of crystalline semiconductor nanowires, Science **279** (5348), 208 (1998).

[65] Y. Cui and C. M. Lieber, Functional nanoscale electronic devices assembled using silicon nanowire building blocks, Science **291** (5505), 851 (2001).

[66] M. S. Gudiksen, L. J. Lauhon, J. Wang, D. C. Smith, and C. M. Lieber, Growth of nanowire superlattice structures for nanoscale photonics and electronics, Nature **415** (6872), 617 (2002).

[67] J. C. Johnson, H. J. Choi, K. P. Knutsen, R. D. Schaller, P. Yang, and R. J. Saykally, Single gallium nitride nanowire lasers, Nature Materials **1** (2), 106 (2002).

[68] Q. Li and G. T. Wang, Spatial distribution of defect luminescence in GaN nanowires, Nano Letters **10** (5), 1554 (2010).

[69] N. Ogasawara and R. Ito, Longitudinal mode competition and asymmetric gain saturation in semiconductor injection lasers. II. Theory, Japanese journal of applied physics **27** (part 1), 615 (1988).

[70] A. Valle, J. Sarma, and K. Shore, Spatial holeburning effects on the dynamics of vertical cavity surface-emitting laser diodes, Quantum Electronics, IEEE Journal of **31** (8), 1423 (1995).

[71] T. Yang, S. Goto, M. Kawata, K. Uchida, A. Niwa, and J. Gotoh, Optical properties of GaN thin films on sapphire substrates characterized by variable-angle spectroscopic ellipsometry, Japanese journal of applied physics **37**, L1105 (1998).

[72] L. Tong, R. R. Gattass, J. B. Ashcom, S. He, J. Lou, M. Shen, I. Maxwell, and E. Mazur, Subwavelength-diameter silica wires for low-loss optical wave guiding, Nature **426** (6968), 816 (2003).

[73] K. Huang, S. Yang, and L. Tong, Modeling of evanescent coupling between two parallel optical nanowires, Applied optics **46** (9), 1429 (2007).

[74] C.-H. Yeh, F.-Y. Shih, C.-T. Chen, C.-N. Lee, and S. Chi, Stabilized dual-wavelength erbium-doped dual-ring fiber laser, Optics Express **15** (21), 13844 (2007).

[75] X. Wu, Y. Sun, J. D. Suter, and X. Fan, Single mode coupled optofluidic ring resonator dye lasers, Applied Physics Letters **94** (24), 241109 (2009).

[76] M. A. Hadley, G. C. Wilson, K. Y. Lau, and J. S. Smith, High single‐transverse‐mode output from external‐cavity surface‐emitting laser diodes, Applied Physics Letters **63** (12), 1607 (1993).

[77] E. W. Young, K. D. Choquette, S. L. Chuang, K. M. Geib, A. J. Fischer, and A. A. Allerman, Single-transverse-mode vertical-cavity lasers under continuous and pulsed operation, Photonics Technology Letters, IEEE **13** (9), 927 (2001).

[78] K. Kieu and M. Mansuripur, Femtosecond laser pulse generation with a fiber taper embedded in carbon nanotube/polymer composite, Optics letters **32** (15), 2242 (2007).

[79] Y. Song, K. Morimune, S. Y. Set, and S. Yamashita, Polarization insensitive all-fiber mode-lockers functioned by carbon nanotubes deposited onto tapered fibers, Applied Physics Letters **90** (2), 021101 (2007).

[80] R. F. Oulton, V. J. Sorger, T. Zentgraf, R. Ma, C. Gladden, L. Dai, G. Bartal, and X. Zhang, Plasmon lasers at deep subwavelength scale, Nature **461** (7264), 629 (2009).

[81] C. Wu, C. Kuo, C. Wang, C. He, M. Lin, H. Ahn, and S. Gwo, Plasmonic Green Nanolaser Based on a Metal–Oxide–Semiconductor Structure, Nano Letters **11** (10), 4256 (2011).

[82] Y. J. Lu, J. Kim, H. Y. Chen, C. Wu, N. Dabidian, C. E. Sanders, C. Y. Wang, M. Y. Lu, B. H. Li, and X. Qiu, Plasmonic Nanolaser Using Epitaxially Grown Silver Film, Science **337** (6093), 450 (2012).

[83] E. D. Palik, *Handbook of optical constants of solids*. (Academic press, 1998).

[84] Y. Ma and L. Tong, Optically pumped semiconductor nanowire lasers, Frontiers of Optoelectronics **5** (3), 239 (2012).

[85] P. A. Williams, Rotating-wave-plate Stokes polarimeter for differential group delay measurements of polarization-mode dispersion, Applied optics **38** (31), 6508 (1999).

[86] T. Grosjean, D. Courjon, and M. Spajer, An all-fiber device for generating radially and other polarized light beams, Optics communications **203** (1), 1 (2002).